Alkynyl Gold(I) Complexes Derived from 3-hydroxyflavones as Multi-Targeted Drugs Against Colon Cancer

Inés Mármol,[a,b] Pilar Castellnou,[a] Raquel Alvarez,[b] M. Concepción Gimeno,[a] M. Jesús Rodriguez-Yoldi,[b] and Elena Cerrada,[a]**

[a]Departamento de Química Inorgánica, Instituto de Síntesis Química y Catálisis Homogénea-ISQCH, Universidad de Zaragoza-C.S.I.C., 50009 Zaragoza, Spain. E-mail: ecerrada@unizar.es

[b]Departamento de Farmacología y Fisiología. Unidad de Fisiología, Universidad de Zaragoza, 50013, Zaragoza, Spain, CIBERobn, IIS Aragón, IA2. E-mail: mjrodyol@unizar.es

Keywords: Alkynyl, gold complexes, hidroxyflavones, thioredoxin reductase, COX, ROS, multi-target

Corresponding author: ecerrada@unizar.es and mjrodyol@unizar.es

Abstract

The design of multi-targeted drugs has gained considerable interest in the last decade thanks to their advantages in the treatment of different diseases, including cancer. The simultaneous inhibition of selected targets from cancerous cells to induce their death represents an attractive objective for the medicinal chemist in order to enhance the efficiency of chemotherapy. In the present work, several alkynyl gold(I) phosphane complexes derived from 3-hydroxyflavones active against three human cancer cell lines, colorectal adenocarcinoma Caco-2/TC7, breast adenocarcinoma MCF-7 and hepatocellular carcinoma HepG2, have been synthesized and characterized. Moreover, these compounds display high selective index values towards differentiated Caco-2 cells, which are considered as a model of non-cancerous cells. The antiproliferative effect of the most active complexes [Au(L2b)PPh_3] (**3b**) and [Au(L2c)PTA] (**4c**) on Caco-2 cells, seems to be mediated by the inhibition of the enzyme cyclooxygenase-1/2 and alteration of the activities of the redox enzymes thioredoxin reductase and glutathione reductase. Both complexes triggered cell death by apoptosis, alterations in cell cycle progression

and increased of ROS production. These results provide support for the suggestion that multi-targeting approach involving the interaction with cyclooxygenase-1/2 and the redox enzymes that increases ROS production, enhances cell death *in vitro*. All these results indicate that complexes [Au(L2b)PPh_3] and [Au(L2c)PTA] are promising antiproliferative agents for further anticancer drug development.

1. Introduction

Cancer chemotherapy based on metallodrugs has been used worldwide, mainly in the case of platinum derivatives, which are active against many tumor types [1]. The activity of platinum-based derivatives (cisplatin, carboplatin, oxaliplatin, etc) is mediated by their ability to form DNA adducts leading to DNA lesions that interfere with transcription and results in cellular death [2]. Regardless of their success in chemotherapy, platinum derivatives produce undesirable side effects and/or acquired resistance that limits their effectiveness [3]. Consequently, the development of novel compounds with metals other than platinum has been growing up during the last decades.

On this regard, gold derivatives and particularly auranofin (1-thio-β-D-glucopyranosatotriethylphosphane gold-2,3,4,6-tetraacetate), have been essayed as biological active products in cancer, neurodegenerative disorders, acquired immunodeficiency syndrome, parasitic and bacterial infection [4]. Moreover, auranofin and related derivatives can reverse important aspects of immune evasion [5]. Additionally, auranofin was approved by FDA (Food and Drug Administration) for the treatment of arthritis rheumatoid in 1985. Consequently, gold compounds would be considered as an alternative to platinum complexes.

Drugs targeting DNA, which is ubiquitously present in cancerous and healthy cells, tend to be more toxic than derivatives with cancer-specific targets. Accordingly, other pharmacological targets of transition metal agents have been investigated, supporting several proteins as important binding partners [6, 7]. Most of the lately approved organic drugs target specific proteins over-expressed or unique to cancer cells [8]. Likewise, the mechanism of gold derivatives is implicated with enzyme inhibition. Thus, auranofin induces apoptosis in cisplatin-resistant cell lines [9], showing a different mechanism of action than cisplatin. Its anticancer activity has been mainly attributed to the inhibition of the enzyme thioredoxin reductase (TrxR) [9-11], which is overexpressed in many cancer cells. Additionally, a second mechanism based in the inhibition of the ubiquitin-proteasome pathway has been also endorsed to auranofin [12, 13]. Interestingly, this

pathway is upregulated in many cancers and several cancer cells have dysfunctional ubiquitin-proteasome system with increased proteasome activity [14]. Thus, gold complexes have been proposed to act as multi-target drugs, which might enhance their clinical effect in comparison to classic platinum-based chemotherapeutic drugs. Multi-targeted compounds are emerging as a therapeutic approach for a variety of cancers [15]. They are able to act on a diverse set of regulatory pathways with a subsequent reduction of systemic toxicities, even addressing resistance issues.

3-Hydroxyflavones (figure 1), also named flavonols are together with flavanols the most common type of flavonoids, being also widely distributed in fruits and vegetables [16, 17]. Quercetin and kaempferol are the most studied and most abundant [18-21]. Many beneficial properties have been endorsed to both that include anti-oxidative activity, anti-inflammatory effects, ameliorative effects against different diseases such as atherosclerosis, thrombosis and arrhythmia, in addition to anticancer properties [22-25]. Their antioxidant power is one of the most known biological properties, being described by several mechanism pathways that includes: ROS inhibition, leukocyte immobilization, nitric oxide inhibition or inhibition of xanthine oxidase [26]. The anti-inflammatory and anticancer properties of phytocompounds seems to be closely related since both have in common the inhibition of the enzyme cyclooxygenase (COX) [27]. COX enzymes are involved in prostaglandin synthesis from arachidonic acid and play a critical role in inflammation and therefore might be related to tumorigenesis. Researchers have traditionally focused on the inhibition of the isoform COX-2, since it is overexpressed on many tumour cells. However, inhibition of the basal isoform COX-1 has also successfully decreased cancer cells proliferation [28].

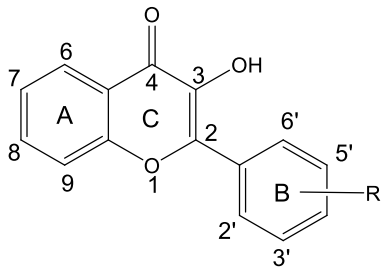

Figure 1. 3-Hydroxyflavone structure.

The presence of the hydroxyl group in C3 position and the keto motif in C4 position enable easy coordination to metal complexes leading to new complexes with biological properties [29-33] .Besides, the –OH group can be functionalized leading to new flavone-

derived ligands with a propargyl ether group able to metal coordination [34]. With this regard and in the particular case of gold, alkynyl derivatives with anticancer properties are less represented in comparison with other organometallic gold complexes, such as N-heterocyclic carbene or cyclometalated compounds [35]. However, the remarkable stability exerted by alkynyl gold species even under physiological conditions, due to the high bond dissociation energy around the gold centre [36], makes them attractive for the development of new metallodrugs.

Thus, we report herein the synthesis of new flavone-derived ligands with a propargyl ether group, the corresponding phosphane gold(I) derivatives and their evaluation against a panel of cancer cells and a model of the intestinal barrier (differentiated Caco-2 cells). To support the hypothesis of multi-target compounds we have studied the effect of some of the new derivatives towards the activity of redox enzymes (thioredoxin reductase and glutathione reductase) along with COX-1/2 enzyme. Measurement of reactive oxygen species (ROS) levels and type of cell death triggered by gold complexes were also investigated.

2. Results and discussion

2.1. Synthesis of ligands.

The synthesis of 3-hydroxyflavones (**HL-1a-d**) was performed in one step, similarly to the previously published method by Ozturk *et al*.[37]. This easy method avoids the isolation of 2-hydroxychalcones, obtained as intermediates, after a Claisen-Schmidt condensation between 2-hydroxyacetophenone and the corresponding benzaldehyde. Flavone-derived ligands (**HL-2a-d**) were synthesized by the base-mediated reaction between 3-hydroxyflavones and propargyl bromide (scheme 1). The formation of the flavone with the propargyl ether group was evidenced by the appearance of a doublet in the ^{1}H NMR spectra characteristic of the methylene unit at around 5 ppm and a triplet for the acetylenic proton at 3.5 ppm ($J_{H\text{-}H} \approx 2.4$ Hz). As occurred in the 3-hydroxyflavones **HL-1a-d** used as precursors, there is a significant difference in the displacements assigned for $H^{3',5'}$ (B ring) in their ^{1}H NMR spectra (see experimental). Thus, electron donating groups, such as *–OMe*, lead to upfield displaced signals while electron withdrawing units drive to downfield displacements.

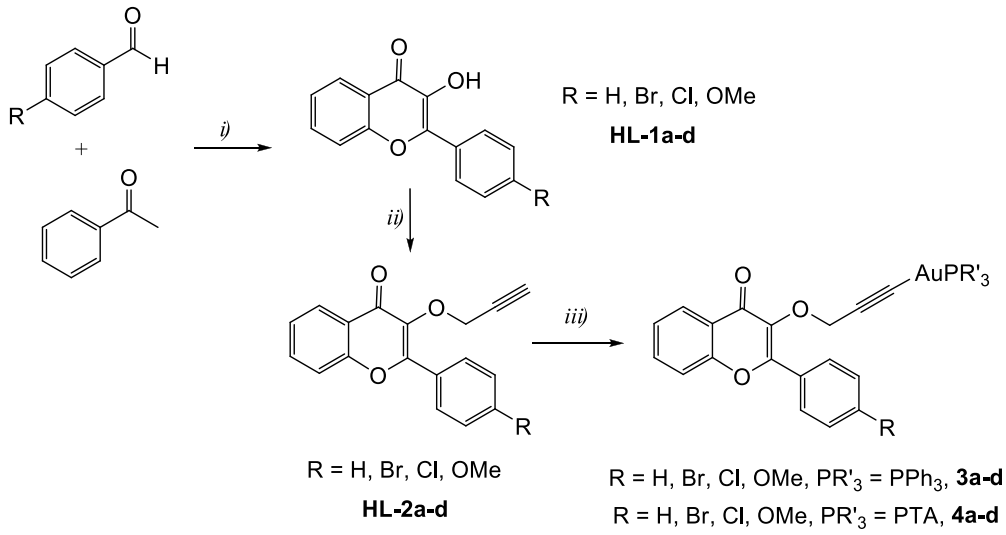

i) NaOH and H_2O_2, *ii)* K_2CO_3 and propargyl bromide, *iii)* KOH/MeOH and [AuClPR'$_3$]

Scheme 1. Preparation of flavones and their gold complexes.

The crystalline structure of **HL-2d** has been established by X-ray analysis (figure 2). The molecule of the flavone presents its typical structure with the aromatic rings in the same plane. The single C-O distances are very dissimilar, the oxygen inside the ring show bond lengths of O3-C11 1.3676(16) and O3-C12 1.3737(16) Å, whereas the oxygen bonded to the propargyl group shows bond lengths of O1-C4 1.3776(17) and O1-C3 1.4524(17) Å, the latter being longer than those to the sp^2 carbon atoms. In a similar manner O4 display distances of O4-C16 1.3645(17) and O4-C19 1.4365(17) Å. The C=O bond distance is O2-C5 1.2366(17) Å, which is typical of a double bond. The propargyl group present C-C distances of C2-C3 1.470(2) and C1 C2 1.186(2) Å, which are typical for single and triple C-C bonds respectively. In the crystal the formation of several secondary bonds such as O···H hydrogen bonds or π-π stacking is observed, which give rise to a three dimensional network structure. The shortest are O4···H-C of 2.718 Å or a slipped π-π stacking of 3.665 Å.

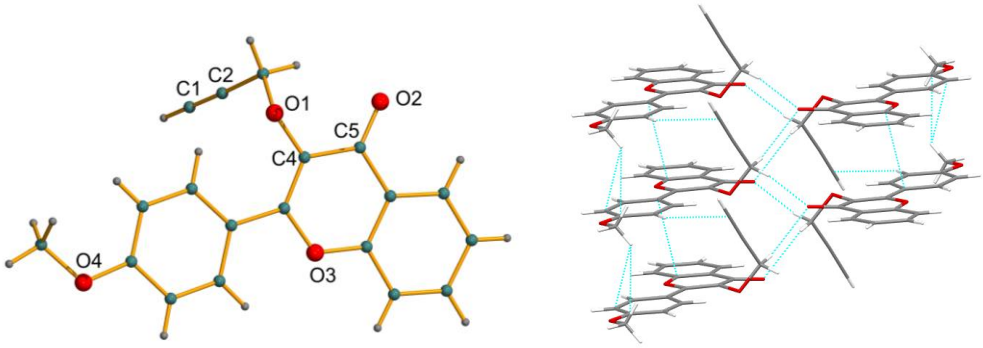

Figure 2. Crystal structure of compound **HL-2d** and part of the three-dimensional network through hydrogen bonding.

2.2. Synthesis of Gold Complexes.

Treatment of the alkyne ligands **HL-2a-d** with [AuCl(PR_3)] (PR_3 = PPh_3 and PTA (PTA = 1,3,5-triaza-7-phosphaadamantane)) in the presence of sodium methoxide afforded the corresponding alkynyl phosphane gold(I) derivatives **3a-d** and **4a-d** (scheme 1) as air-stable solids. The disappearance of the acetylenic triplet and the downfield shift of the methylene signal in their ^{1}H NMR spectra are indicative of gold coordination. The spectra of complexes **3a-d** display a more complicated pattern in comparison to their precursors, as a consequence of the presence of the PPh_3 in the aromatic region. Similar spectroscopic data are observed for complexes **4a-d** to those of their precursors, in addition to the AB system and a singlet at 4.2 ppm characteristics of the NCH_2N and NCH_2P moieties of the PTA molecule respectively. The $^{31}P\{^{1}H\}$ NMR spectra show one resonance at around +41 ppm in the case of the triphenylphosphane derivatives and at about -49 ppm for PTA complexes. In addition, their infrared spectra also display changes in the ν(C≡C) vibration in comparison to the alkyne flavones. The free ligands exhibit a stretching vibration of C≡C as a weak band at 2110 cm^{-1}, which is slightly displaced to around 2130 cm^{-1} in the gold complexes, and a narrow band around 3200 cm^{-1} due to the terminal alkyne (≡C-H) stretch, which disappears once coordinated to the gold phosphane units.

2.3. Solution Stability.

The stability of the complexes was analysed by UV-vis absorption spectroscopy in PBS solution (PBS buffer at pH = 7.4). Solutions suitable for spectrophotometric analysis were prepared by diluting dimethylsulfoxide (DMSO**)** mother solutions of the complexes with PBS buffer. The resulting solutions were monitored over 24 h at 37 ºC. The spectra of the complexes show intense absorption bands at ca. 210 nm and two lower energy absorption bands with low intensity in the region of 250-320 nm, which could be assigned as $\pi \rightarrow \pi^*$ intraligand transitions of the alkynyl ligands (Figure S38). The higher energy absorption band around 210 nm is also tentatively assigned to the intraligand transition characteristic of triphenylphosphane, as similar absorption bands are also observed in related Au(PPh_3) complexes [38]. In all the complexes the transitions remain without any changes in shape or displacement in the absorbance maximum (none apparent red- or blue shift), in addition to lacking of absorbance at around 500 nm (characteristic of gold reduction) over 24 h, implying a substantial stability of the chromophore under physiological conditions.

2.4. Lipophilicity.

On the basis of Lipinski's rule, lipophilicity and hydrophilicity are essential on the performance of drug research. High lipophilicity or high hydrophilicity can hinder biomedical applications [39]. Consequently, a balanced relationship between lipophilicity and hydrophilicity would be important in drug delivery process.

The balance between lipophilicity and hydrophilicity can be measured by the partition coefficient water/n-octanol, *logP,* by experimental procedures such as the shake flask method, which studies the distribution of the drug between an equal amount of n-octanol and water (or buffered aqueous solution) [40]. Our alkynyl gold(I) derivatives display values of *logP* (at pH = 7.4) in the range 0.23 to 1.2 (Table 2), being higher in the cases of the triphenylphosphane compounds that implies higher lipophilicity in comparison with the PTA counterparts.

Flavonoids are highly lipophilic compounds, being therefore difficult their oral bioavailability. Consequently, alternative routes of administration have been explored for their delivery, such as the use of nanoparticles, lipid nanocapsules, microparticle or microsponges as delivery systems [41]. The functionalisation of the flavone with the propargyl ether moiety and the subsequent coordination of the

gold-phosphane unit, has resulted in a decrease of their lipophilic character and a balanced relationship between lipophilicity and hydrophilicity.

2.5. Bovine Serum Albumin Interaction.

Considering that the majority of chemotherapeutic treatments use bloodstream for drug transport and that blood plasma proteins are able to interact with the drug, we have studied the interaction of some of the new complexes with albumin.

Bovine serum albumin (BSA) is frequently used as a model protein for HSA (human serum albumin) due to their similarity and commercial availability [42].

The interaction of the alkynyl gold derivatives with BSA has been studied by the addition of increasing amounts of the complexes to a solution of BSA followed by the measurement of the quenching of BSA fluorescence emission, due to the tryptophan residues, upon excitation at 295 nm. No emission was observed for the gold compounds in the range 310-400 nm.

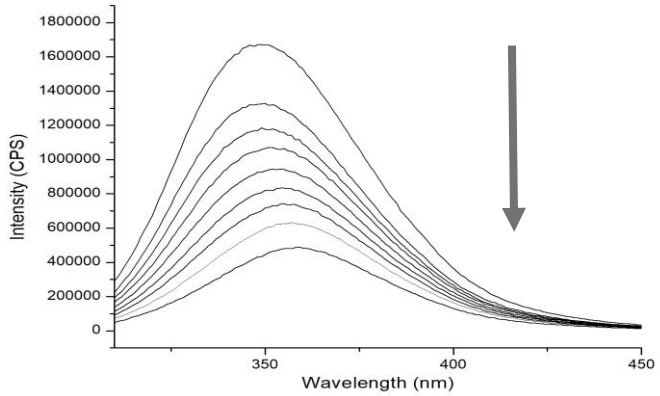

Figure 3. Fluorescence emission spectra of BSA at 298 K in the presence of different concentrations of [Au(L2a)PTA] (**4a**) Arrow indicates the increase of the quencher concentration (0-30 μM).

A concentration dependent quenching of the fluorescence is observed, lacking changes in shape and a slight displacement in the position of the maximum (*ca*. 6-8 nm) has been observed (see figure 3 as example). Fluorescence data were analysed by the Stern-Volmer equation (see supplementary material) and the corresponding plot F_0/F *vs* [complex] (F and F_0 are the corresponding intensities in the presence and the absence of the quencher agent) gives a linear plot (Figure 4A and figure S40) in the cases of complexes **3a**, **3b** and **4b**, characteristic of the presence of a single mechanism of quenching, static or dynamic [43]. However,

complexes **3c**, **4a**, **4c** and **4d** give a plot with a positive deviation (concave towards the *y* axis), which suggests the presence of a combination of static and dynamic quenching by the fluorophore.

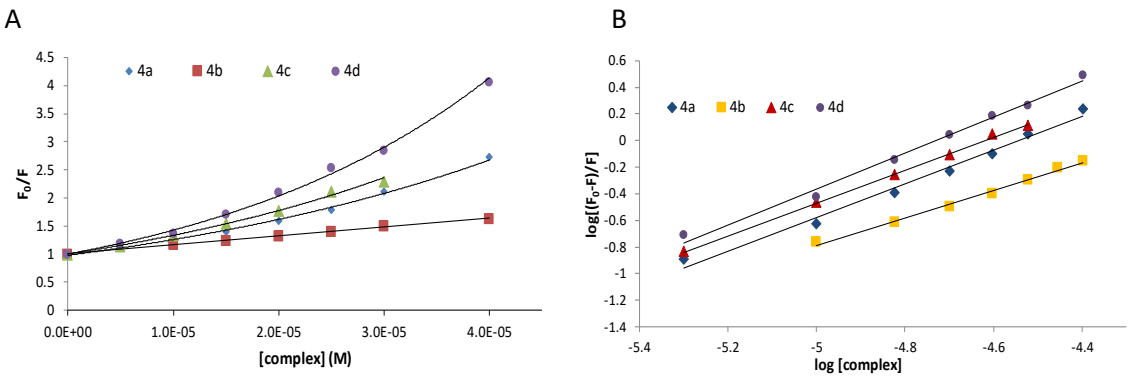

Figure 4. Stern-Volmer plots for the quenching of BSA with increasing amounts of PTA complexes (complex concentration from 0 μM to 40 μM) at 298 K (λ_{exc} = 295 nm, [BSA] = 50 μM). A) Stern-Volmer equation used: $F_0/F = 1 + K_{sv}$[complex]. The slope of the best fit linear trend provides the Stern-Volmer quenching constant K_{sv} for PTA complexes. B) Stern-Volmer equation used: $\log\{(F_0\text{-}F)/F\} = \log K_b + n\log$[complex]. The intercept of the best fit linear trend provides the Stern-Volmer quenching constant K_b.

The quenching of the emission can be quantified only in the cases of linear representation of the plot F_0/F *vs* [complex]. Thus, complexes **3a**, **3b** and **4b** afford a quenching constant value (K_{sv}) in the order of $1x10^4$ M^{-1} (Table 1). The value of the bimolecular quenching constant, k_q, which represents the efficiency of quenching or how accessible the fluorophores are to the quencher, can afford an idea of the type of quenching mechanism. Thus, a k_q value higher than the diffusion-controlled rate constant of the biomolecule in water, 10^{10} $M^{-1}s^{-1}$, could indicate some type of binding interaction implying a possible contribution of static quenching, since a dynamic quenching depends on diffusion. k_q calculated (K_{sv}/τ_0 by using the standard value of 10^{-8} s for τ_0) in the case of complexes **3a**, **3b** and **4b** afford a value of *ca.* 10^{12}, pointing to a static quenching rather than dynamic quenching.

Analysis of the absorption spectra of the fluorophores can also be useful to characterize static and dynamic quenching. In view of implication of complex formation in a static quenching, changes in the absorption spectra of BSA could be expected; whereas these spectra would remain unchanged in a dynamic quenching, since only excited states of BSA are affected. BSA displays two absorption peaks

at around 210 nm, which represents the content of α-helix in the protein and at 280 nm, which arises from π→π* transition of aromatic amino acid residues [44].

Table 1. Values of Stern-Volmer quenching constant (K_{sv}), the number of binding sites and the apparent binding constant (K_b) for the interaction of complexes with BSA and with BSA-Ibuprofen or BSA-Phenylbutazone for complex **4d**.

System	K_{sv} (M^{-1})	K_b (M^{-1})	*n*
BSA-[Au(L2a)PPh_3] (**3a**)	3.05×10^4	3.74×10^5	1.24
BSA-[Au(L2b)PPh_3] (**3b**)	5.67×10^4	1.41×10^5	1.08
BSA-[Au(L2c)PPh_3] (**3c**)	-	1.22×10^5	1.14
BSA-[Au(L2a)PTA] (**4a**)	-	5.19×10^5	1.25
BSA-[Au(L2b)PTA] (**4b**)	1.77×10^4	2.45×10^4	1.03
BSA-[Au(L2c)PTA] (**4c**)	-	4.95×10^5	1.23
BSA-[Au(L2d)PTA] (**4d**)	-	2.35×10^6	1.34
BSA-Ibuprofen-**4d**	-	4.47×10^4	1.02
BSA-Phenylbutazone-**4d**	-	2.04×10^6	1.37

Addition of increasing amounts of [Au(L2b)PTA] (**4b**) to a solution of BSA (10 μM in PBS) (figure 5) resulted in a decrease of the absorbance intensity at 280 nm (saturation taking place beyond 40 μM) that suggest an interaction of the complex and the protein, probably as a consequence of a conformational change. Similar results have been described with other drugs [45].

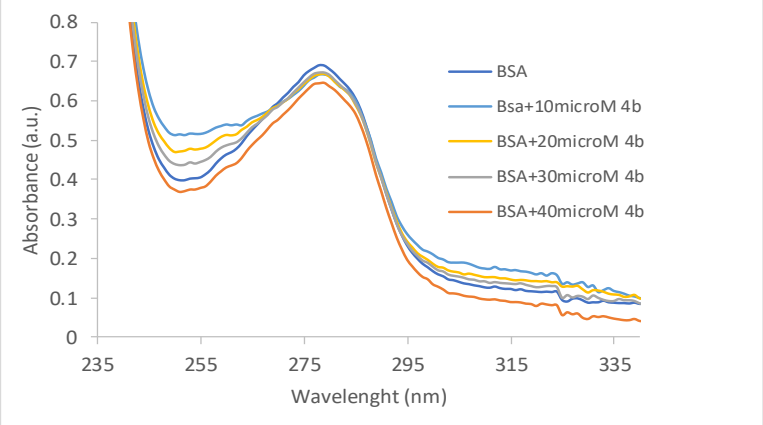

Figure 5. UV-visible absorption spectra of BSA with increasing amounts of [Au(L2b)PTA] (**4b**) at 298K. [BSA = 10 μM] and [**4b**] (10-50μM). Equal concentration of **4b** was also added to the reference cell (in each measurement) in order to eliminate its absorbance.

Dynamic quenching does not affect the absorption of quenching molecule as only affects its excited states, consequently the changes observed in the spectrum could

be indicative of static quenching. The absorption spectra of the rest of the complexes in a 1:1 stoichiometry gave also a decrease of the BSA absorption, in accordance with the presence of a static quenching mechanism (see supplementary material).

Fluorescence intensity data has allowed us to calculate the values of the binding constant for each experiment and the number of binding sites by means of the representation of log (F_0-F/F) *versus* log[complex] (Figure 4B and figure S41). The binding constant values (summarized in Table 1) are in the range 2.4 x 10^4 to 2.3 x 10^6 M^{-1}. These values are in agreement with those observed for dithiocarbamate gold(III) derivatives [46] and for [Au(C≡CPh)(PTA)] [47], although higher than other alkynyl or thiolate phosphane gold(I) complexes previously reported by us.[48-53].

The main molecule binding sites of BSA are located in the subdomain IIA and IIIA, commonly named as sites I and II [54]. Site I shows affinity for warfarin, phenylbutazone, etc. meanwhile site II is well suited for ibuprofen, diazepam, etc [55]. In order to localize our derivatives, we have performed displacement experiments with ibuprofen and phenylbutazone as site markers. Complex **4d**, with the highest binding constant value, was added in increasing amounts to a mixture of BSA with ibuprofen or BSA with phenylbutazone and monitored the emission intensity quenching (see figures S42-S46). The emission data were analysed similarly than the above described experiments. As a result, the new binding constant (Table 1) is affected in the presence of ibuprofen, since its value has decreased remarkably, while the addition of phenylbutazone maintained its value in the same order. This result indicates that complex **4d** competes with ibuprofen in subdomain IIA and its binds in site I of BSA.

2.6. Biological Studies.

2.6.1. Analysis of the Antiproliferative Effect

The toxicity of 3-hydroxyflavones and flavone-derived ligands was firstly evaluated on undifferentiated Caco-2/TC7 cells by two different methods: sulforhodamine B (SRB) and MTT (Table 2). Some authors have reported that flavone-containing molecules such as polyphenols might interfere with MTT assay. On the one hand, polyphenols might trigger an increase in the activity of the mitochondrial dehydrogenase enzyme, which would lead to an enhanced reduction of MTT that not truly correlates with cell proliferation. Additionally, polyphenols

are able to reduce MTT to formazan themselves, leading to false positive [56]. Therefore, alternatives to MTT assay are recommended to the evaluation of the antiproliferative effect of plant-derived molecules, including DNA-based methods and the sulforhodamine B assay.

Table 2. IC_{50} (μM)[a] values of 3-hydroxyflavones and flavone-derived ligands on undifferentiated Caco-2/TC7.

Compound	Assay method	
	MTT	SRB
HL-1a	89.1± 4.98	16.7 ± 8.28
HL-1b	22.0 ± 0.25	10.4 ± 0.24
HL-1c	16.5 ± 0.69	13.5 ± 0.33
HL-1d	22.3 ± 2.51	14.8 ± 2.82
HL-2a	63.56 ± 17.87	54.87 ± 2.05
HL-2b	> 100	65.64 ± 38.92
HL-2c	39.09 ± 30.98	27.19 ± 3.02
HL-2d	64.14 ± 13.95	49.07 ± 3.84

[a]Mean ± SE of at least three determinations

When comparing the IC_{50} values of the four 3-hydroxyflavones **HL1a-d** obtained by SRB and MTT (Table 2), we found that SRB method provided values 1.2 to 5 times lower than the MTT technique, which might be indicative of slight interference with the second procedure. Furthermore, the obtained IC_{50} values of flavone-derived ligands **HL2a-d** were significantly higher when determined by MTT than with SRB; in addition, results obtained with MTT assay were found to be less reproducible since higher standard error values were found. We concluded that SRB was a more reliable technique to evaluate the antiproliferative effect of 3-hydroxyflavones and flavone-derived ligands. However, such interferences with the MTT assay were not observed for the eight gold derivatives at concentrations below 20 μM except for [Au(L2d)PPh_3] (**3d**) (Figure S49). All complexes were tested by both assay techniques on undifferentiated Caco-2/TC7 cells at a range of concentrations (from 1.25 to 20 μM). The resulting dose-response curves and the IC_{50} values obtained with the SRB technique and MTT assay (Tables S1 and 3 respectively) were comparable. We hypothesized that the interaction between flavone-containing molecules and the MTT assay -and the subsequent false positives- were strongly influenced by concentration; thus, MTT was considered

as an adequate assay procedure when incubation with gold derivatives was performed at concentration values below 20 μM.

Cytotoxicity of the eight novel gold derivatives was also evaluated on breast adenocarcinoma MCF-7 and hepatocellular carcinoma HepG2 in addition to colorectal adenocarcinoma Caco-2 (TC7 clone). To further determine the selectivity of the complexes, differentiated Caco-2 cells were used as a model of the intestinal barrier. As can be observed on Table 3, all complexes reduced cell proliferation on each cancer cell line analysed and the obtained IC_{50} values were lower than the ones of 3-hydroxyflavones and flavone-derived ligands. These results suggest that coordination of the gold phosphane unit to flavones enhances their natural antiproliferative effect and leads to more efficient chemotherapeutic drugs.

Table 3. Distribution coefficients and IC_{50} (μM)[a] values of the complexes on undifferentiated Caco-2/TC7, MCF-7 and HepG2 cancer cell lines and on differentiated Caco-2 cells (non-cancerous model) compared with auranofin and cisplatin.

Compound	$logD_{7.4}$	Caco-2/TC7	MCF-7	HepG2	Dif Caco-2
[Au(L2a)PPh_3] (**3a**)	0.99	3.81 ± 1.18	2.08 ± 0.17	32.34 ± 4.27	131.30 ± 38.54
[Au(L2b)PPh_3] (**3b**)	0.92	1.52 ± 0.91	13.87 ±0.78	3.38 ± 0.07	43.89 ± 0.02
[Au(L2c)PPh_3] (**3c**)	1.17	5.34 ± 0.05	8.99 ± 3.89	34.14 ± 5.88	114.38 ± 9.24
[Au(L2d)PPh_3] (**3d**)	1.2	4.78 ± 0.62	3.40 ± 0.85	47.97 ± 5.32	75.45 ± 11.28
[Au(L2a)PTA] (**4a**)	0.78	7.68 ± 1.74	18.49 ± 0.90	10.84 ± 0.67	18.25 ± 1.34
[Au(L2b)PTA] (**4b**)	0.80	6.42 ± 0.35	8.80 ± 3.14	11.25 ± 0.63	24.39 ± 0.86
[Au(L2c)PTA] (**4c**)	0.23	2.33 ± 1.26	7.57 ± 0.08	5.88 ± 0.04	25.46 ± 0.66
[Au(L2d)PTA] (**4d**)	0.44	5.22 ± 0.43	9.19 ± 2.89	10.70 ± 1.35	25.29 ± 0.60
Cisplatin	-0.53	37.24 ± 5.15	41.82 ± 0.07	49.85 ± 6.66	151.13 ± 58.12
Auranofin	-2.53	1.80 ± 0.1	0.77 ± 0.05	0.92 ± 0.08	6.21 ± 0.44

[a] Mean ± SE of at least three determinations by using MTT method

Undifferentiated Caco-2/TC7 cells showed a better response to treatment with all complexes than MCF-7 and HepG2 cells. The IC_{50} values obtained on undifferentiated Caco-2/TC7 and MCF-7 cells were significantly lower when compared to cisplatin. Auranofin, on the other hand, displayed a higher antiproliferative effect on the three cancer cell lines than our compounds in most of the cases, although the IC_{50} values of complexes [Au(L2b)PPh_3] (**3b**) (1.52 ± 0.91 μM) and [Au(L2c)PTA] (**4c**) (2.33 ± 1.26 μM) were comparable to the obtained upon treatment with auranofin (1.80 ± 0.10 μM) on undifferentiated Caco-2 cells. Whereas the IC_{50} values of the PTA gold derivatives (complexes **4a, 4b, 4c**

and **4d**) on HepG2 cells were comparable to the measured on Caco-2 and MCF-7, the cytotoxicity of the related PPh_3 derivatives against HepG2 cells was 3 to 4 times lower, except for [Au(L2b)PPh_3] (**3b**), which indeed displayed an IC_{50} value 3.33 times higher than the PTA counterpart **4b**. Curiously, the opposite effect was observed on MCF-7 cell line, in which complex **3b** displayed the highest IC_{50} value compared with the other three PPh_3 complexes. In general, similar IC_{50} values were observed in related alkynyl gold(I) phosphane complexes on MCF-7 or Caco-2 cells [35, 50, 51, 57-60].

Caco-2 cell line is considered a model of the intestinal barrier due to the spontaneous differentiation acquired after reaching confluence. Therefore, we tested the toxicity of the series of gold derivatives on differentiated Caco-2 cells in order to obtain a first estimation in regard to their behaviour on non-cancerous tissue (Table 3), and the Selectivity Index (SI) was in addition calculated (Table S1) as previously indicated by Badisa *et al.*[61]. Whereas the SI values of the PTA complexes were in the same range than the obtained for cisplatin and auranofin on the three cancer models, PPh_3 derivatives highlighted due to their high selectivity to undifferentiated Caco-2 cells, with SI values 5 to 10 times higher than those obtained for cisplatin and auranofin. Complexes **3a**, **3c** and **3d** showed in addition higher SI values than cisplatin and auranofin on MCF-7. Finally, [Au(L2b)PPh_3] (**3b**) was the only complex to display a remarkably higher SI value than cisplatin (4.3-up fold) and auranofin (1.92-up fold). To further analyse the toxicity of our complexes on a non-cancerous model, differentiated Caco-2 cells were incubated 72h with the complexes at the IC_{50} values previously obtained on undifferentiated Caco-2 cells (Figure S51). No significant changes in cell viability were observed, with suggests that these concentration values resulted toxic on cancerous cells rather than on the non-cancerous ones.

According to the results obtained on this section in terms of antiproliferative effect and selectivity on cancer cells, [Au(L2b)PPh_3] (**3b**) and [Au(L2c)PTA] (**4c**) were selected as the most promising complexes and their mechanism of action on undifferentiated Caco-2/TC7 cells was further analysed.

2.6.2. Measurement of COX-1/2 Activity

Given the affinity of flavones for the enzyme cyclooxygenase (COX), [62, 63] we considered both isoforms 1 and 2 as likely targets of our flavone gold derivatives [Au(L2b)PPh_3] (**3b**) and [Au(L2c)PTA] (**4c**). Therefore, we measured the activity

of COX-1 (Figure 6.A) and COX-2 (Figure 6.B) from undifferentiated Caco-2/TC7 cells after 2 and 24h of incubation. A reduction of the activity of the enzyme COX-1 is observed along the first 2h of incubation with both complexes. However, non-inhibitory effect was detected after overnight incubation with complex **3b**. Nevertheless, in the case of complex **4c**, inhibition of COX-1 was noticed at both incubation periods, being 16.3 times lower after 24h of incubation. Our data suggest that cellular compensation mechanisms might be occurring, although further assays are needed to validate this hypothesis. Regarding to the enzyme COX-2, [Au(L2b)PPh_3] (**3b**) significantly decreased its activity at 2h that was maintained after 24h of incubation, whereas treatment with [Au(L2c)PTA] (**4c**) did not display any effect on COX-2 activity. Therefore, these results suggest that **3b** and **4c** might interact with different targets.

Few research data are available in regards to the inhibitory effect of COX triggered by gold complexes. Auranofin was recently reported to be able to inhibit COX-2 [64]. In addition, Ott *et al*. reported its ability for COX-1 inhibition in human platelets [65], although authors evaluated high concentrations (10 and 100 μM) that according to our data on differentiated Caco-2 cells (Table 2) would be considerably cytotoxic for non-cancerous tissue. However, gold coordination to 3-hydroxyflavones might increase its affinity for this enzyme, leading to stronger anticancer and anti-inflammatory properties. Similar results have been obtained with drugs containing well-known COX inhibitors including valdecoxib [66] and acetylsalicylic acid [67] among others.

Although inhibition of both isoforms 1 and 2 has been related to antitumor effect, inhibition of COX-2 is preferred due to the minor incidence of side effects. COX-1 is involved on gastric mucosa maintenance and its pharmacological inhibition is related to gastric injury.[68] Therefore, researchers have focused on the development of novel selective COX-2 inhibitors. In line with this, the absence of inhibitory effect of COX-1 activity after 24h incubation with complex **3b** is of great interest since it might be indicative of COX-2 selectivity and consequently might induce less side effects than complex **4c**.

The different effect induced on COX-1/2 activity by complexes **3b** and **4c** might explain the results obtained on MCF-7 cell line. As shown in Table 2, [Au(L2b)PPh_3] (**3b**) displayed less toxicity on this cell model in comparison with undifferentiated Caco-2 and HepG2, whereas the IC_{50} values of [Au(L2c)PTA] (**4c**)

were comparable between the three cell lines. Contrary to HepG2 [69] and Caco-2 [70], MCF-7 human breast tumor cell line lacks endogenous COX-2 expression [71]. Consequently, the reduced antitumor effect of complex **3b** on MCF-7 cells is not surprising since at least one of its targets is absent. Furthermore, these results suggest that complex **3b** might be a multi-target compound, given that it displays toxicity on MCF-7 despite the lack of the enzyme COX-2.

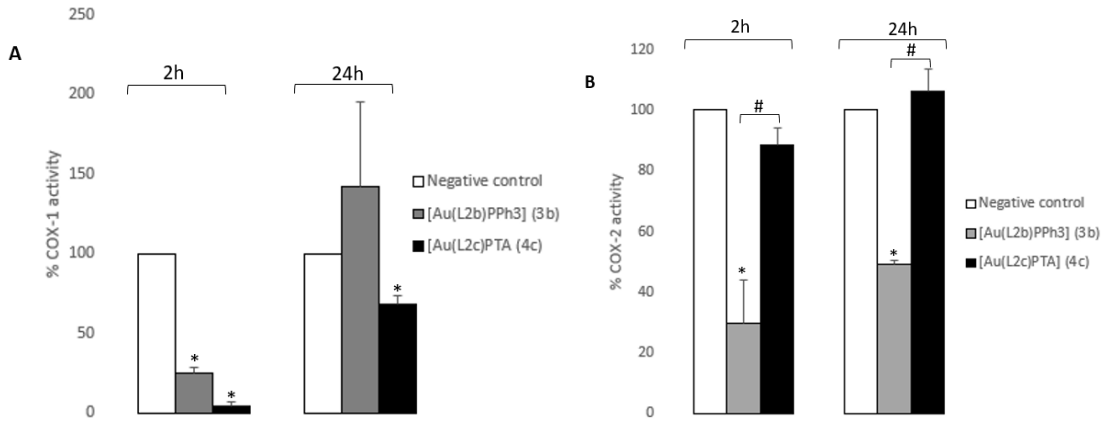

Figure 6. Measurement of COX activity. A) Determination of COX-1 activity from undifferentiated Caco-2/TC7 cells after 2 and 24h incubation with [Au(L2b)PPh_3] (**3b**) and [Au(L2c)PTA] (**4c**) at their IC_{50} values. B) Determination of COX-2 activity from undifferentiated Caco-2/TC7 cells after 2 and 24h incubation with [Au(L2b)PPh_3] (**3b**) and [Au(L2c)PTA (**4c**) at their IC_{50} values. *p<0.05 *vs* negative control. #p<0.05 *vs* gold complex.

2.6.3. Analysis of Redox Enzymes TrxR and GR Inhibition

Most of gold complexes are able to interact with Thioredoxin reductase due to the affinity between the gold atom and the selenocysteine residue present on the active site of the enzyme [72, 73]. Less data has been collected in regards to the interaction between gold derivatives and glutathione reductase (GR), which has also a key role in controlling redox balance [74]. The function of GR and TrxR are closely related and the inhibition of any of them leads to cancer cell death due to an aberrant increase in ROS levels. Misfunction of one of these systems might lead to overcompensation of the other in order to avoid cell failure [75, 76]. Furthermore, authors have reported that certain flavanols are able to directly inhibit TrxR [77] and GR [78]. Therefore, we investigated the influence of [Au(L2b)PPh_3] (**3b**) and [Au(L2c)PTA] (**4c**) on the activity of TrxR (Figure 7.A) and GR (Figure

7.B) from undifferentiated Caco-2/TC7 cells after 2 and 24h of incubation with the complexes.

As shown in Figure 7.A, both complexes [Au(L2b)PPh_3] (**3b**) and [Au(L2c)PTA] (**4c**) were able to inhibit TrxR activity after short incubation time (2h), which was maintained upon overnight treatment. Indeed, after 24h incubation we observed a higher decrease in TrxR activity induced by complex **4c**, whereas the effect caused by complex **3b** remained unchanged. Regarding to interaction with GR (Figure 7.B), complex **3b** did not induce any changes after 2h incubation, whereas a great increase in GR activity was noticed after 24h of incubation. According to previous results from Jortzik *et al*. [79], inhibition of TrxR induced by gold complexes might lead to upregulation of the expression of those enzymes involved in both thioredoxin and glutathione systems in order to restore redox balance. Our present data suggest that inhibition of TrxR triggered by complex **3b** leads to a compensatory overexpression of GR. On the other hand, complex **4c** effectively inhibited GR activity although initially the activity of the enzyme was increased in comparison to negative control. In conclusion, herein we have demonstrated that complex **3b** inhibits TrxR, thus leading to an increase in GR activity, whereas complex **4c** was found able to inhibit both TrxR and GR after 24h incubation. Taken together, these results and our previous findings regarding to the effect on COX-1/2 activity, our gold complexes seem to act through a multi-target mechanism of action.

Villegas *et al*. [80] found that COX-1 inhibition with piroxicam resulted in glutathione (GSH) depletion along with a decrease in GR activity on a rat gastric mucosa. Although COX-2 selective inhibition eventually resulted in the same situation, treatment with piroxicam triggered GSH depletion in a faster manner. We have also observed an interplay between COX-1 and GR inhibition on undifferentiated Caco-2 cells treated with [Au(L2c)PTA] (**4c**). Since inhibition of COX-1 was noticed previously to the decrease in GR activity, it is feasible to suggest that the inhibition of GR induced upon treatment with complex **4c** might be a consequence of direct inhibition of the enzyme, a downstream event of COX-1 inhibition or a combination of both. Future assays are needed.

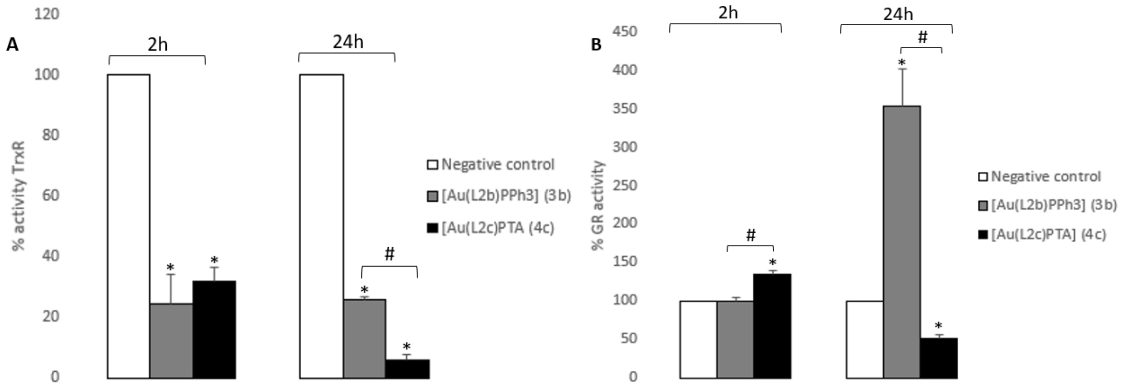

Figure 7. Analysis of the activity of redox enzymes. A) Measurement of the activity of TrxR from undifferentiated Caco-2/TC7 cells after 2 and 24h of incubation with [Au(L2b)PPh_3] (**3b**) and [Au(L2c)PTA] (**4c**) at their IC_{50} values. B) Measurement of the activity of GR from undifferentiated Caco-2/TC7 cells after 2 and 24h incubation with [Au(L2b)PPh_3] (**3b**) and [Au(L2c)PTA] (**4c**) at their IC_{50} values. *$p<0.05$ *vs* negative control. #$p<0.05$ *vs* gold complex.

2.6.4. Determination of ROS levels

As aforementioned, inhibition of TrxR and GR has been related to a dramatic increase in ROS levels that triggers cell death [81]. In light of this, we measured ROS production on undifferentiated Caco-2/TC7 cells incubated with [Au(L2b)PPh_3] (**3b**) and [Au(L2c)PTA] (**4c**) for 1, 3 and 24h (Figure 8).

Treatment with both complexes resulted in an increased ROS generation upon overnight incubation. According to results obtained after 1 and 3h incubation respectively, the pro-oxidant effect of [Au(L2b)PPh_3] (**3b**) was slightly faster than the induced by [Au(L2c)PTA] (**4c**). Similar increase in ROS and reduction of thioredoxin reductase activity have been found in gold(I) and gold(III) derivatives [47, 82]. As previously shown on Figure 7, although both complexes **3b** and **4c** are able to inhibit TrxR after 2h incubation, treatment with **4c** induced initially an increase in GR activity. Therefore, despite complex **4c** triggered a greater decrease in TrxR than complex **3b** at short incubation time, the increased activity of GR maintained redox balance and no significant changes in ROS levels were observed at 1h of incubation. Moreover, some authors have reported that inhibition of COX-2 lead to a overproduction of ROS [83, 84]. Thus, the observed effect on ROS production induced by [Au(L2b)PPh_3] (**3b**) might be a consequence of the

inhibition of both TrxR and COX-2, which could explain the significant ($p<0.05$) increase in ROS levels after 1h incubation.

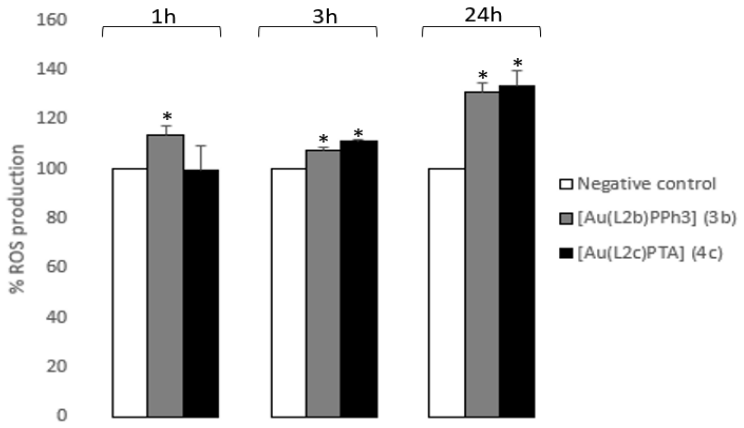

Figure 8. Time-course (1, 3 and 24h) measurement of ROS generation on undifferentiated Caco-2/TC7 cells upon incubation with [Au(L2b)PPh_3] (**3b**) and [Au(L2c)PTA (**4c**) at their IC_{50} values. *$p<0.05$ *vs* negative control.

2.6.5. Cell Death Studies

Once it has been evaluated the mechanism of action of the multi-target complexes [Au(L2b)PPh_3] (**3b**) and [Au(L2c)PTA (**4c**), we analyzed the type of cell death triggered by both of them.

We found that [Au(L2b)PPh_3] (**3b**) induced apoptosis on Caco-2/TC7 after 24h incubation at its IC_{50} concentration (Figure 9). As shown in Figure 9.A, total apoptotic events increased a 5.9-up fold after treatment with complex **3b**, with a significant increase in late apoptotic population in comparison with negative control. Moreover, an increase in the number of cells undergoing early apoptosis were also noticed, although it was statistically non-significant. Contrarily, no significant changes in the percentage of cells undergoing necrosis were noticed (Figure S52). Induction of apoptosis was further confirmed by the observed increase in the percentage of cells with activated caspase 3 (Figure 9.B).

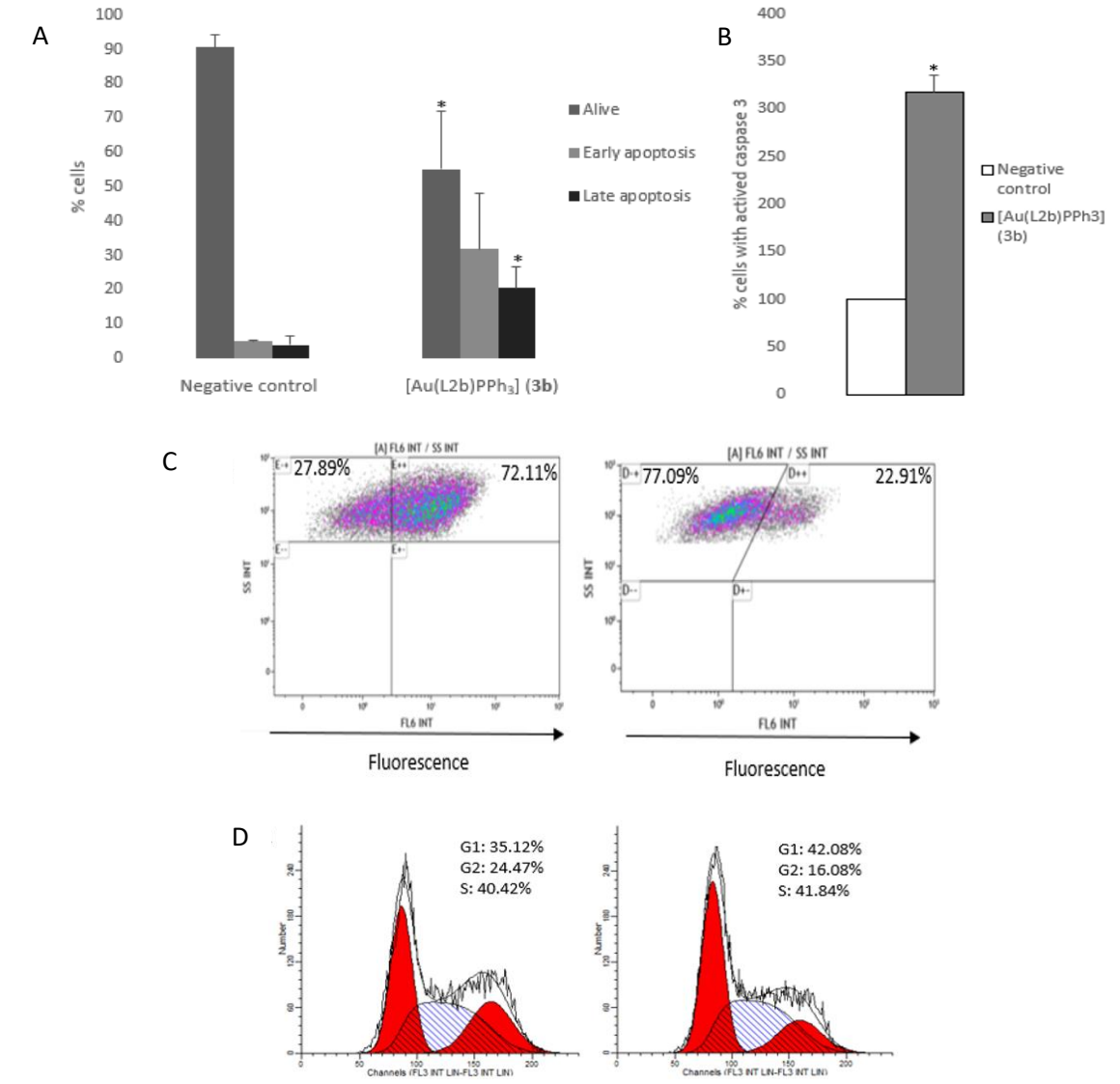

Figure 9. Analysis of the type of cell death induced on undifferentiated Caco-2/TC7 cells after 24h incubation with [Au(L2b)PPh$_3$] (**3b**) at its IC_{50} value. A) Percentages of alive, necrotic, early apoptotic and late apoptotic cells. B) Percentages of cells with activated caspase 3. C) Analysis of the integrity of mitochondrial membrane potential in terms of loss of fluorescence. Percentages of each cell population are included. D) Cell cycle analysis. Percentages of each cell population are included. *p<0.05 *vs* negative control

Gold complexes are known to preferentially trigger mitochondrial or intrinsic apoptosis rather than by extrinsic pathway. One of the most relevant steps of intrinsic apoptosis is the loss of mitochondrial membrane potential (MMP) that leads to the eventual collapse of the whole organelle. The analysis of mitochondrial integrity upon 24h incubation with complex **3b** was performed by measuring the incorporation of the cationic dye DiIC1 (1, 1',3,3,3'-haxamethylindodicarbo-

cyanine iodide). As can be observed in Figure 9.C, complex **3b** increased the percentage of cells with altered MMP when compared with untreated cells, which might be indicative of the induction of mitochondrial apoptosis.

The pro-apoptotic effect of complex **3b** lead to alterations in cell cycle progression, which produced a reduction in G_2 population concomitant to an increase in number of cells undergoing G_1 phase, similarly to auranofin [85] (Figure 9.D)

On the other hand, [Au(L2c)PTA] (**4c**) did not display any significant changes in apoptotic population after 24h incubation, although a 8.5-up fold increase in late apoptotic cells population was detected after 48h of incubation (Figure 10.A). The delay in apoptosis induction compared to [Au(L2b)PPh_3] (**3b**) might be related to the previously discussed slower pro-oxidant effect (Figure 8), given the key role of redox homeostasis on cancer cell survival. Nevertheless, the antiproliferative effect of [Au(L2c)PTA] (**4c**) after overnight incubation was enhanced by pre-incubation with the autophagy inhibitor chloroquine (CQ) (Figure 10.B). Due to the aberrant proliferation of cancer cells, increased basal rates of autophagy have been found in comparison to non-cancerous cells, and in the concrete case of colorectal cancer (CRC) upregulation of autophagy is related to tumour mass growth and spread.

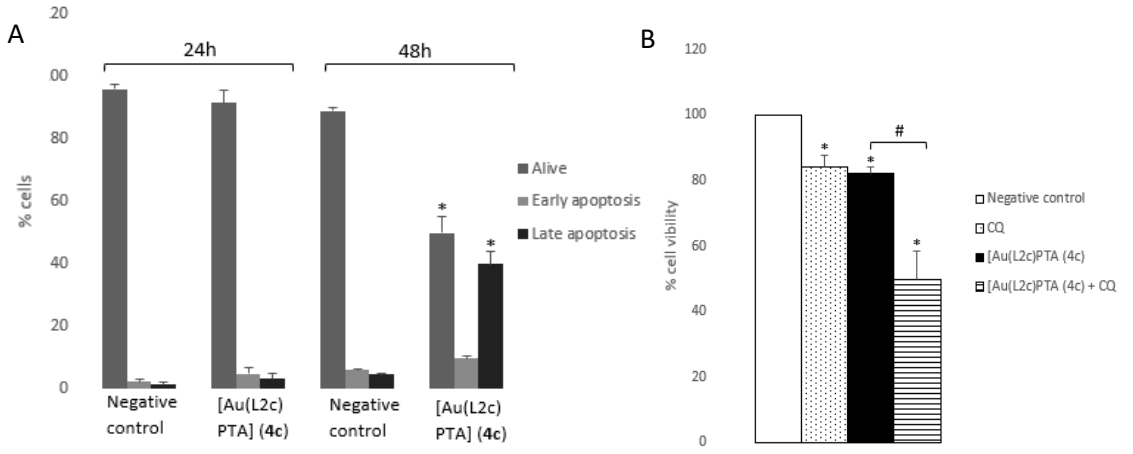

Figure 10. Analysis of cell death induced on undifferentiated Caco-2/TC7 cells after incubation with [Au(L2c)PTA] (**4c**) at its IC_{50} value. A) Time-dependent effect of apoptosis induction after 24 and 48h incubation of undifferentiated Caco-2/TC7 cells with [Au(L2c)PTA] (**4c**) at its IC_{50} value. B) Effect of pre-incubation with chloroquine (10 μM, 1h) on changes in undifferentiated Caco-2/TC7 cells viability upon 24h treatment with [Au(L2c)PTA]. *p<0.05 *vs* negative control. #p<0.05 *vs* gold complex.

Moreover, autophagy is closely related to prognosis, since it can lead to drug resistance and chemotherapy failure [86]. Consequently, the therapeutic modulation of autophagy has been proposed as a novel approach to CRC treatment in order to increase chemosensitivity. Shi *et al*. [87] found that pre-treatment of Caco-2 cells with the autophagy inhibitor 3-methyladenine resulted in an enhancement of cell sensitivity to oxaliplatin. Our present findings demonstrate that the chemotherapeutic potential of autophagy inhibition is not limited to platinum-based drugs since gold complexes can also be benefited from this strategy.

3. Conclusions

In this work, the synthesis of new flavone-derived ligands with a propargyl ether group, the corresponding alkynyl gold(I) derivatives and the evaluation of their anticancer activity is described. The complexes are stable at 37 ºC under physiological conditions, display balanced relationship between lipophilicity and hydrophilicity and good binding propensity to BSA, being the hydrophobic cavity of site I in the subdomain IIA of BSA the most probable location of the gold complex. Although free flavones are active against Caco-2/TC7 human colon cancer cells, a large enhancement of the cytotoxicity has been obtained after gold(I) coordination. In addition, such coordination has allowed the interaction of the gold complexes with COX-1/2 enzyme as well as with the redox enzymes TrxR and GR, which leads to an increased ROS production on colorectal adenocarcinoma cell line Caco-2. Through a multi-targeted mechanism of action, these series of gold complexes have triggered apoptotic cell death *via* the intrinsic pathway and have altered cell cycle progression. Moreover, toxicity evaluation on differentiated Caco-2 cells as a model of non-cancerous tissue suggests that these gold complexes might act preferentially on cancer cells rather than on the differentiated ones. Finally, preliminary studies showed that the concomitant administration of [Au(L2c)PTA] with autophagy inhibitors such as chloroquine might enhance its antiproliferative effect due to the blockage of cytoprotective autophagy. Taken together, our results suggest a promising future for these complexes on cancer chemotherapy.

4. Experimental

4.1. General procedure for the preparation of the 3-hydroxyflavones [37] (**HL-1a-d**). NaOH (0.4 g) was added to a methanol (20 mL) solution of 2-hydroxyacetophenone (3.32 mmol) and benzaldehyde or the different *para*-substituted benzaldehydes (3.32 mmol).

The reaction was refluxed for 3 h until it acquires an intense orange color. The reaction was cooled to room temperature and followed by the addition of NaOH (0.4 g) dissolved in 20 mL of water and 1.45 mL of H_2O_2 (33% w/v). After 3 h of stirring, the mixture was poured into an ice-water solution affording yellow solids, which were filtered off and dried in air.

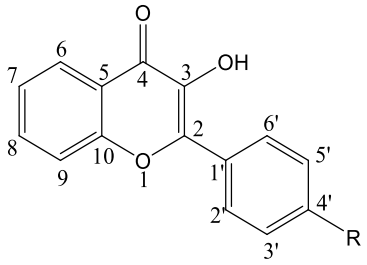

2-phenyl-3-hydroxy-4H-chromen-4-one (**HL-1a**, R = H). Yellow solid in 58% yield. ^{1}H NMR (400 MHz, dmso-d_6, 25ºC) δ (ppm) = 8.69 (m, 2H, $H^{2',6'}$), 8.02 (dd, J = 8.1 Hz; 1.2 Hz 1H, H^6), 7.56 (m, 2H, H^9+H^8), 7.37 (dd, J = 10.7; 5.0 Hz, 2H, $H^{5',3'}$), 7.24 (ddd, 8.0; 6.6; 1.4 Hz, 1H, H^7), 7.16 (dd, J = 10.7; 4.2 Hz, 1H, $H^{4'}$). ^{13}C{^{1}H} NMR (100 MHz, $CDCl_3$): δ (ppm) = 177.3 (C=O), 154.5 (C^3), 144.4 (C^2), 134.0, 132.6 ($C^{7,9}$), 128.5 ($C^{3',5'}$), 128.0 (C^8), 126.6 ($C^{2',6'}$), 125.2 (C^6), 123.7 ($C^{4'}$), 121.7, 118.7 ($C^{7,9}$). IR: ν(-OH) 3385cm^{-1}, ν(C=O) 1519cm^{-1}.

2-(4-bromophenyl)-3-hydroxy-4H-chromen-4-one (**HL-1b**, R = Br). Yellow solid in 67% yield. ^{1}H NMR (400 MHz, dmso-d_6, 25ºC) δ (ppm) = 8.65 (d, J = 8.0 Hz; 2H, $H^{2',6'}$), 8.00 (m, 1H, H^6), 7.56 (m, 2H, H^9+H^8), 7.51 (d, J = 8.9 Hz, 2H, $H^{5',3'}$), 7.22 (ddd, J = 6.8; 5.8; 2.2 Hz, 1H, H^7). ^{13}C{^{1}H} NMR (100 MHz, $CDCl_3$): δ(ppm) = 180.3 (CO), 156.2 ($C^{4'}$), 143.0, 133.6, 132.6 ($C^{8,9}$), 131.4 ($C^{3',5'}$), 128.1 ($C^{2',6'}$), 125.3 (C^6), 123.6 (C^7), 121.5, 120.4, 118.6 ($C^{8,9}$). IR: ν(-OH) 3335cm^{-1} , ν(C=O) 1624cm^{-1}.

2-(4-clorophenyl)-3-hydroxy-4H-chromen-4-one (**HL-1c**, R = Cl). Yellow solid in 62% yield. ^{1}H NMR (400 MHz, dmso-d_6, 25ºC) δ (ppm) = 8.73 (d, J = 8.6 Hz, 2H, $H^{2'6'}$), 8.00 (m, 1H, H^6), 7.56 (dt, J = 8.5; 5.0 Hz, 2H, $H^{9,8}$), 7.39 (d, J = 8.9 Hz, 2H, $H^{5',3'}$), 7.23 (ddd, J = 8.0; 6.2, 1.8 Hz, 1H, H^7). ^{13}C{^{1}H} NMR (100 MHz, $CDCl_3$): δ(ppm) 177.9 (C=O), 154.4 ($C^{4'}$), 154.1, 142.3 (C^3, C^2), 134.8 (C^6), 131.6 (C^9), 129.9, 128.1 ($C^{3',5'}$), 126.7 ($C^{2',6'}$), 125.3, 122.7 (C^7), 121.7, 118.4 (C^8). IR: ν (-OH) 3351 cm^{-1}, ν (C=O) 1594 cm^{-1}.

2-(4-metoxiphenyl)-3-hydroxy-4H-chromen-4-one (**HL-1d**, R = OCH_3). Yellow solid in 59% yield. ^{1}H NMR (400 MHz, dmso-d_6, 25ºC) δ (ppm) = 8.66 (d, J = 9.1 Hz, 2H, $H^{2',6'}$), 8.01 (dd, J = 8.0; 1.2 Hz, 1H, H^6), 7.54 (ddd, J = 12.2; 10.1; 4.7 Hz , 2H, $H^{9,8}$), 7.24 (m,

2H, $H^{5',3'}$), 6.95 (d, J = 9.1Hz, 1H, H^{7}). $^{13}C\{^{1}H\}$ NMR (100 MHz, $CDCl_3$): δ(ppm) 176.6 (C=O), 159.3($C^{4'}$), 154.3, 145 (C^{3}), 132.3 ($C^{8,9}$), 128.4 ($C^{2',6'}$), 126.5, 125.1 (C^{6}), 123.7 (C^{7}), 121.7, 118.52 ($C^{8,9}$), 114.9 ($C^{3',5'}$), 114.0, 55.6 (-OCH_3). IR: ν (-OH) 3195 cm^{-1}, ν (C=O) 1595 cm^{-1}

4.2. General procedure for the preparation of the propargyl flavones **HL-2a-d.** K_2CO_3 in excess and propargylbromide (1.6 equivalents) were added to a solution of flavones HL-1a-d. The reaction was heated under reflux for 6 hours, and after this time, the excess of base was filtered off and the residue was evaporated to dryness.

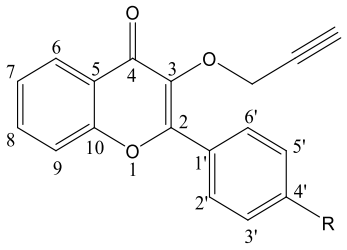

*2-phenyl-3-(prop-2-in-1-yloxy)-4H-chromen-4-one (**HL-2a**, R = H). White solid in* 50% yield. ^{1}H NMR (400 MHz, dmso-d_6, 25ºC) δ (ppm) = 8.12 (m, 3H, H^{6} + $H^{2',6'}$), 7.86 (ddd, J = 8.5; 6.9; 1.6 Hz, 1H,H^{8}), 7.79 (m, 1H, H^{9}), 7.59 (m, 3H, $H^{3',4',5'}$), 7.53 (m, 1H, H^{7}), 4.98 (d, J = 2.4 Hz, 2H, -CH_2-), 3.48 (t, J = 2,4 Hz, 1H, -C≡C-H). $^{13}C\{^{1}H\}$ NMR (100 MHz, CDCl3): δ(ppm) = 176.6 (C=O), 156.4, 155.2, 138.4, 134.4 (C^{8}), 131.4, 130.8, 129.1, 129.1, 125.7 ($C^{2',3',4',5',6'}$), 125.4 (C^{7}), 123.7 (C^{6}), 118.9 (C^{9}), 79.7 y 79.1 (C≡C), 59.1 (-$C$$H_2$). IR: ν(≡C-H) 3253 cm^{-1}, ν(C≡C) 2113 cm^{-1}, ν(C=O) 1611cm^{-1}. Elemental analysis calcd. (%) for $C_{18}H_{12}O_3$ (276.28): C 78.25, H 4.38; found: C 77.88, H 4.26.

2-(4-bromophenyl)-3-(prop-2-in-1-yloxy)-4H-chromen-4-ona (**HL-2b**, R = Br). White solid in 52% yield. ^{1}H NMR (400 MHz, dmso-d_6, 25ºC) δ (ppm) = 8.11 (m, 1H, H^{6}), 8.07 (m, 2H, $H^{2',6'}$), 7.88 (d, J = 8.0 Hz, 1H, H^{8}), 7.81 (d, J = 8.0Hz, 3H, H^{9}+$H^{3',5'}$), 7.53 (ddd, J = 8.0; 7.0; 1.1 Hz, 1H, H^{7}), 4.98 (d, J = 2.5 Hz, 2H, -CH_2-), 3.48 (t, J = 2,5 Hz,1H, -C≡C-H). ^{13}C $\{^{1}H\}$ NMR (100 MHz, $CDCl_3$): δ(ppm) = 174.1 (C=O), 154.9 and 155.3 ($C^{3,5}$), 138.3 ($C^{4'}$), 134.7 (C^{7}), 131.2 and 131.3 ($C^{2',6'}$ and $C^{3',5'}$), 130 (C^{1}'), 125.8 and 125.3 ($C^{6,8}$), 124.9 and 123.9 ($C^{10,2}$), 118.8 (C^{9}), 79.9 and 78.9 (C≡C), 59.2 *(-CH_2-).* IR: ν(≡C-H) 3228 cm^{-1}, ν(C≡C) 2117 cm^{-1}, ν(C=O) 1605 cm^{-1}. Elemental analysis calcd. (%) for $C_{18}H_{11}BrO_3$ (355.18): C 60.87, H 3.12; found: C 60.52, H 3.13.

2-(4-clorophenyl)-3-(prop-2-in-1-yloxy)-4H-chromen-4-one (**HL-2c,** R = Cl). White solid in 50% yield. ^{1}H NMR (400 MHz, dmso-d_6, 25ºC) δ (ppm) = 8.14 (t, J = 6.4 Hz,

2H, $H^{2',6'}$), 8.10 (dd, J = 8.0; 1.4 Hz, 1H, H^{6}), 7.87 (m, 1H, H^{8}), 7.79 (d, J = 8.0 Hz , 3H, H^{9} +$H^{3'5'}$), 7.65 (d, J = 8.7 Hz, 1H, H^{7}), 4.98 (d, J = 2.4 Hz, 2H, -CH_2-), 3.46 (m, 1H, -$C{\equiv}C$-H). $^{13}C\{^1H\}$ NMR (100 MHz, $CDCl_3$): δ(ppm) = 174.2 (C=O), 155.1 ($C^{3,5}$), 138.2, 134.8 ($C^{8,9}$), 130.9 ($C^{2',6'}$), 129.1 ($C^{3',5'}$), 125.8, 125.4, 123.7 (C^{7}), 118.8 ($C^{9,8}$), 79.9 and 79.0 ($C{\equiv}C$), 59.25 *(-CH_2-)*. IR: ν(≡C-H) 3238 cm^{-1}, ν(C≡C) 2112 cm^{-1}, ν(C=O) 1628 cm^{-1}. Elemental analysis calcd. (%) for $C_{18}H_{11}ClO_3$ (310.73): C 69.58, H 3.57; found: C 69.24, H 3.75.

2-(4-metoxiphenyl)-3-(prop-2-in-1-yloxy)-4H-chromen-4-one (**HL-2d**, R = OMe). White solid in 52% yield. ^1H NMR (400 MHz, dmso-d_6, 25ºC) δ (ppm) = 8.17 (m, 2H, $H^{2',6'}$), 8.11 (m, 1H, H^{6}), 8.09 (dd, J = 8.0; 1.4 Hz, 1H, H^{8}), 7.84 (m, 1H, H^{9}), 7.77 (d, J = 7.8 Hz, 3H, $H^{3',5'}$), 7.50 (m, 1H, H^{7}), 4.96 (d, J = 2.4Hz, 2H, -CH_2-), 3.86 (s, 3H, OMe), 3.46 (s, 1H, -C≡CH). $^{13}C\{^1H\}$ NMR (100 MHz, $CDCl_3$): δ(ppm) = 174.7(C=O), 161.6 ($C^{4'}$), 156.7 and 155.2 ($C^{3,5}$), 138.0 ($C^{1'}$), 133.3 (C^{8}), 130.7($C^{2',6'}$), 125.7 and 124.7 ($C^{6,8}$), 124.0 and 123.7 ($C^{10,2}$), 117.9 (C^{9}), 113.8 ($C^{3',5'}$), 78.7 and 75.9 ($C{\equiv}C$), 59.25 *(-CH_2-)*, 55.4 (OCH_3). IR: ν(≡C-H) 3286 cm^{-1}, ν(C≡C) 2161 cm^{-1}, ν(C=O) 1634 cm^{-1}. Elemental analysis calcd. (%) for $C_{19}H_{14}O_4$ (306.31): C 74.50, H 4.61; found: C 74.15, H 4.85

4.3. Synthesis of the [Au(L2)PR'$_3$] complexes. To a solution of KOH (0.225 mmol) in MeOH (ca. 10 mL) containing **L2a-d** (0.15 mmol) was added [AuCl(PR'$_3$)] (PR'$_3$ = PPh_3, PTA) (0.15 mmol). The gold derivatives [AuCl(PPh_3)] and [AuCl(PTA)] were prepared as published elsewhere [88, 89]. The corresponding solids precipitated in the methanolic solution, and were isolated by filtration after 20 h of stirring at room temperature, washed with methanol and diethyl ether, and dried in *vacuo*. Using this method, the following complexes were prepared:

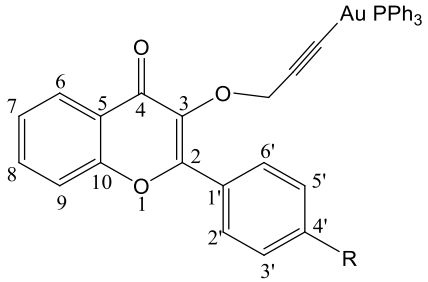

[Au(L2a)PPh_3] (**3a**). Yield: 65%. White solid. ^1H NMR (400 MHz, dmso-d_6) δ(ppm) = 8.27 (m, 2H, $H^{2',6'}$), 8.20 (dd, J = 8.1, 1.4Hz, 1H, H^{6}), 7.92 (ddd, J = 8.4; 7; 1.6Hz, 1H, H^{7}), 7.85 (d, J = 8.0Hz, 1H, H^{9}), 7.62 (m, 19H, PPh_3 +$H^{3',4',5'}$+H^{8}), 5.08 (s, 2H, -CH_2-) $^{31}P\{^1H\}$ NMR (162 MHz, dmso-d_6) δ(ppm): 41.4 (s). $^{13}C\{^1H\}$ NMR (100 MHz, $CDCl_3$): δ(ppm) = 175.2 (C=O), 156.7, 155.3, 139.3, 134.2 (d, J = 13.9 Hz, C_{orto}, PPh_3), 133.1,

131.5 (d, *J* = 2.2 Hz, C_{para}, PPh_3), 130.3, 130.1, 129.4, 129.2, 129.1 (d, *J* = 11.3 Hz, C_{meta}, PPh_3), 128.2, 125.9, 124.4, 124.3, 117.9, 98.2 and 98.7 (*C*≡*C*), 60.7 *(-CH_2-).* IR: ν(C≡C) 2136cm^{-1}, ν(C=O) 1626cm^{-1}. Elemental analysis calcd. (%) for $C_{36}H_{26}AuO_3P$ (734.53): C 58.87, H 3.57; found: C 58.52, H 3.4.

[Au(L2b)PPh_3] (**3b**). Yield: 65%. White solid. ^{1}H NMR (400 MHz, dmso-d_6) δ(ppm) = 8.13 (m, 3H, $H^{2',6'}$+H^6), 7.85 (ddd, *J* = 8.4, 7.2, 1.6Hz, 1H, H^7), 7.75 (m, 3H, $H^{3',5'}$+H^9), 7.54 (m, 16H, PPh_3+H^8), 4.98 (s, 2H, -CH_2-). ^{31}P{^{1}H} NMR (162 MHz, dmso-d_6) δ(ppm): 41.3 (s). ^{13}C{^{1}H} NMR (100 MHz, $CDCl_3$): δ(ppm) = 175.0 (*C*=*O*), 155.7, 155.2, 139.3, 134.2 (d, *J* = 13.9 Hz, C_{orto}, PPh_3), 133.3, 131.5 (d, *J* = 2.4 Hz, C_{para}, PPh_3), 131.4, 130.8, 130.5, 130.0, 129.8, 129.3, 129.1 (d, *J* = 11.3 Hz, C_{meta}, PPh_3), 125.9, 124.9, 124.6, 124.2, 117.9, 98.3 and 97.9 (*C*≡*C*), 60.8 *(-CH_2-).* IR: ν(C≡C) 2130cm^{-1}, ν(C=O) 1631cm^{-1}. Elemental analysis calcd. (%) for $C_{36}H_{26}AuClO_3P$ (813.43): C 53.16, H 3.10; found: C 52.85, H 2.9.

[Au(L2b)PPh_3] (**3c**). Yield: 65%. White solid. ^{1}H NMR (400 MHz, dmso-d_6) δ(ppm) = 8.22 (m, 2H, $H^{2',6'}$), 8.11 (dd, *J* = 7.8, 1.6Hz, 1H, H^6), 7.85 (ddd, *J* = 8.4, 6.8, 1.6Hz, 1H, H^7), 7.77 (d, *J* = 8Hz, 1H, H^9), 7.54 (m,18H, PPh_3+$H^{3',5'}$+H^8), 4.99 (s, 2H, -CH_2-). ^{31}P{^{1}H} NMR (162 MHz, dmso-d_6) δ(ppm): 41.3 (s). ^{13}C{^{1}H} NMR (100 MHz, $CDCl_3$): δ(ppm) = 173.7 (*C*=*O*), 152.2, 134.2 (d, *J* = 13.6 Hz, C_{orto}, PPh_3), 133.6, 132.1, 130.7, 129.3 (d, *J* = 11.3 Hz, C_{meta}, PPh_3), 128.5, 125.6, 118.5, 97.4 and 96.9 (*C*≡*C*), 60.5 *(-CH_2-).* IR: ν(C≡C) 2130cm^{-1}, ν(C=O) 1625cm^{-1}. Elemental analysis calcd. (%) for $C_{36}H_{26}AuClO_3P$ (768.97): C 56.23, H 3.28; found: C 55.90, H 3.04.

[Au(L2b)PPh_3] (**3d**). Yield: 71%. White solid. ^{1}H NMR (400 MHz, dmso-d^6) δ(ppm) = 8.20 (d, *J* = 8.6Hz, 2H, $H^{2',6'}$), 8.09 (d, *J* = 7.63Hz, 1H, H^6), 7.79 (m, 2H, $H^{9,7}$), 7.52 (m, 16H, PPh_3+H^8), 7.10 (d, *J* = 8.6 Hz, 2H, $H^{3',5'}$), 4.97 (s, 2H, -CH_2-), 3.81 (s, 3H, -CH_3) ^{31}P{^{1}H} NMR (162 MHz, dmso-d_6) δ(ppm): 41.2 (s). ^{13}C{^{1}H} NMR (100 MHz, $CDCl_3$): δ(ppm) = 174.8 (*C*=*O*), 161.3, 155.2, 134.2 (d, *J* = 13.9 Hz, C_{orto}, PPh_3), 132.5, 131.5 (d, *J* = 2.2 Hz, C_{para}, PPh_3), 130.9, 130.1, 129.4, 129.1 (d, *J* = 11.3 Hz, C_{meta}, PPh_3), 125.9, 124.3, 123.9, 117.8, 113.7, 98.3 and 98.7 (*C*≡*C*), 60.6 *(-CH_2-)*, 55.3 (O*Me*). IR: ν(C≡C) 2130cm^{-1}, ν(C=O) 1627cm^{-1}. Elemental analysis calcd. (%) for $C_{37}H_{28}AuO_4P$ (764.56): C 58.12, H 3.69; found: C 57.85, H 3.54.

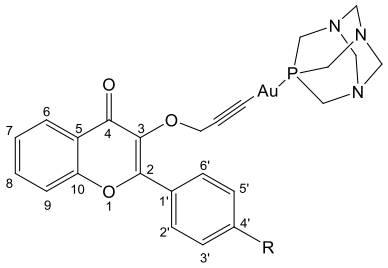

[Au(L2a)PTA] (**4a**). Yield: 55%. Light yellow solid. ^{1}H NMR (400 MHz, dmso-d$_6$) δ(ppm) = 8.17 (m, 2H, $H^{2',6'}$), 8.10 (d, *J* = 6.9 Hz, 1H, H^{6}), 7.84 (d, *J* = 7.5Hz, 1H, H^{7}), 7.78 (d, *J* = 8.5Hz, 1H, H^{9}), 7.54 (m, 4H, $H^{3',5'}$+H^{4}+H^{8}), 4.99 (s, 2H, -CH_2-), 4.44 and 4.31 (AB system, *J* = 12.0Hz, 6H, NCH_2N), 4.18 (s, 6H, NCH_2P). ^{31}P*{^{1}H}* NMR (162 MHz, dmso-d$_6$) δ(ppm): -49.2 (s). ^{13}C{^{1}H} NMR (100 MHz, $CDCl_3$): δ(ppm) = 174.8 (*C=O*), 156.4, 155.3, 139.1, 133.2, 131.3, 130.4 (C^{9}), 129.0 and 128.3 ($C^{3',5'}$ and $C^{2',6'}$), 125.9 (C^{6}), 124.5 (C^{8}), 124.2, 117.9 (C^{7}), 98.6 (*C≡C*), 73.2 (d, *J* = 6.9 Hz, *NCH_2N*), 60.6 *(-CH_2-)*, 52.3 (d, *J* = 20 Hz, *NCH_2P*). IR: ν(C≡C) 2136cm^{-1}, ν(C=O) 1630cm^{-1}. Elemental analysis calcd. (%) for $C_{24}H_{23}AuN_3O_3P$ (629.39): C 45.80, H 3.68, N 6.68; found: C 45.50, H 3.71, N 6.50

[Au(L2b)PTA] (**4b**). Yield: 55%. Light yellow solid. ^{1}H NMR (400 MHz, dmso-d$_6$) δ(ppm) = 8.11 (m, 3H, $H^{2',6'}$+H^{6}), 7.84 (d, *J* =7.1Hz, 1H, H^{7}), 7.78 (m, 3H, $H^{3',5'}$+H^{6}), 7.52 (t, *J* = 7.3Hz, 1H, H^{8}), 4.98 (s, 2H, -CH_2-), 4.44 and 4.31(AB system, *J* = 12.0Hz, 6H, NCH_2N), 4.18 (s, 6H, NCH_2P). ^{31}P*{^{1}H}* NMR (162 MHz, dmso-d$_6$) δ(ppm): -49.4 (s). ^{13}C{^{1}H} NMR (100 MHz, dmso-d$_6$): δ(ppm) = 174.4 (*C=O*), 155.1, 138.7, 134.7, 131.9 and 131.1 ($C^{3',5'}$ and $C^{2',6'}$), 130.4, 125.7, 125.4, 124.9, 123.7, 118.9, 87.2 (*C≡C*), 72.2 (d, *J* = 7.7 Hz, *NCH_2N*), 60.6 *(-CH_2-)*, 51.1 (d, *J* = 20 Hz, *NCH_2P*). IR: ν(C≡C) 2120cm^{-1}, ν(C=O) 1627cm^{-1}. Elemental analysis calcd. (%) for $C_{24}H_{22}AuBrN_3O_3P$ (708.29): C 40.69, H 3.13, N 5.93; found: C 40.38, H 2.83, N 5.88

[Au(L2c)PTA] (**4c**). Yield: 60%. Light yellow solid. ^{1}H NMR (400 MHz, dmso-d$_6$) δ(ppm) = 8.20 (d, *J* = 8.7Hz , 2H, $H^{2',6'}$), 8.10 (d, *J* = 6.7Hz, 1H, H^{6}), 7.84 (d, *J* = 6.9Hz, 1H, H^{7}), 7.78 (d, *J* = 8.4Hz, 1H, H^{9}),7.65 (d, *J* = 8.7Hz, 2H, $H^{3',5'}$), 7.52 (t, *J* = 7.4 Hz, 1H, H^{8}), 4.98 (s, 2H, -CH_2-), 4.44 and 4.31 (AB system, *J* = 12.0Hz, 6H, NCH_2N), 4.17 (s, 6H, NCH_2P). ^{31}P{^{1}H} NMR (162 MHz, dmso-d$_6$) δ(ppm): -49.2 (s). ^{13}C{^{1}H} NMR (100 MHz, dmso-d$_6$): δ(ppm) = 174.5 (*C=O*), 155.1, 138.7, 135.9, 134.7, 130.9 and 128.9 ($C^{3',5'}$ and $C^{2',6'}$), 130.0, 125.7, 125.4, 123.7, 118.9, 99.7 (*C≡C*), 72.2 (d, *J* = 8.2 Hz, *NCH_2N*), 60.5 *(-CH_2-)*, 51.3 (d, *J* = 21.2 Hz, *NCH_2P*). IR: ν (C≡C) 2122cm^{-1}, ν(C=O)

1628cm^{-1}. Elemental analysis calcd. (%) for $C_{24}H_{22}AuClN_3O_3P$ (663.84): C 43.42, H 3.32, N 6.33; found: C 43.07, H 2.98, N 6.72

[Au(L2d)PTA] (**4d**). Yield: 65%. Light yellow solid. ^{1}H NMR (400 MHz, dmso-d$_6$) δ(ppm) = 8.18 (d, *J* = 8,7 Hz, 2H, $H^{2',6'}$), 8.08 (d, *J* = 8.5Hz, 1H, H^6), 7.82 (d, *J* = 7.7Hz, 1H, H^7), 7.76 (d, *J* = 8.5Hz, 1H, H^9), 7.51 (t, *J* = 7.0Hz, 1H, H^8), 7.12 (d, *J* = 8.7Hz, 2H, $H^{3',5'}$), 4.97 (s, 2H, -CH_2-), 4.44 and 4.31 (AB system, *J* = 12.0Hz, 6H, NCH_2N), 4.18 (s, 6H, NCH_2P). ^{31}P{^{1}H} NMR (162 MHz, dmso-d$_6$) δ(ppm): -49.1 (s). ^{13}C{^{1}H} NMR (100 MHz, dmso-d$_6$): δ(ppm) = 173.7 (*C*=*O*), 161.2, 155.6, 155.1, 134.3, 130.9 and 114.4 ($C^{3',5'}$ and $C^{2',6'}$), 125.5, 125.3, 123.7, 118.8, 93.3 (*C*≡*C*), 72.2 (d, *J* = 7.7 Hz, *NCH$_2$N*), 60.3 *(-CH$_2$-)*, 55.9 (O*Me*), 51.5 (d, *J* = 20 Hz, *NCH$_2$P*). IR: ν(C≡C) 2123cm^{-1}, ν(C=O) 1600cm^{-1}. Elemental analysis calcd. (%) for $C_{25}H_{25}AuN_3O_4P$ (659.42): C 45.54, H 3.82, N 6.37; found: C 45.18, H 3.71, N 5.98

4.4. Crystal Structure Determination: Crystals were mounted in inert oil on glass fibres and transferred to the cold gas stream of a Smart APEX CCD diffractometers equipped with a low-temperature attachment. Data were collected using monochromated MoKα radiation (λ = 0.71073 Å). Scan type ϖ. Absorption corrections based on multiple scans were applied using SADABS. The structures were solved by direct methods and refined on F^2 using the program SHELXL-2016 [90]. All non-hydrogen atoms were refined anisotropically. CCDC 1922088 contains the supplementary crystallographic data for this paper. These data can be obtained free of charge via www.ccdc.cam.ac.uk/data_request/cif, or by emailing data_request@ccdc.cam.ac.uk, or by contacting The Cambridge Crystallographic Data Centre, 12 Union Road, Cambridge CB2 1EZ, UK; fax: +44 1223 336033.

4.5. Cell culture. Human colorectal adenocarcinoma Caco-2 cells were kindly provided by Dr. Edith Brot-Laroche (Université Pierre et Marie Curie-Paris 6 UMR S872, Les Cordeliers, France). Human breast adenocarcinoma MCF-7 cells were kindly provided by Carlos J. Ciudad and Dr. Verònica Noé (Departamento de Bioquímica y Fisiología, Facultad de Farmacia, Universidad de Barcelona, Spain). Human hepatocellular carcinoma HepG2 cells were kindly provided by Dr. María Angeles Alava (Departamento de Bioquímica y Biología Molecular, Universidad de Zaragoza, Spain). All cell lines were maintained in a humidified atmosphere of 5% CO_2 at 37ºC. Cells (passages 20-40) were grown in Dulbecco's Modified Eagles medium (DMEM) (Gibco Invitrogen, Paisley, UK) supplemented with 20% fetal bovine serum, 1% non-essential amino acids, 1% penicillin (1000 U/mL), 1% streptomycin (1000 μg/mL) and 1% amphotericin (250 U/mL). Culture

medium was replaced every two days and cells were passaged enzymatically with 0.25% trypsin-1 mM EDTA and sub-cultured on 25 cm^2 flasks at a density of $2 \cdot 10^4$ cells/cm^2. Experiments in undifferentiated Caco-2 cells as well as on MCF-7 and HepG2 cells were performed 24h post-seeding. For assays on differentiated Caco-2 cells, cells were cultured on 96-wells plates under standard culture conditions for 7 to 9 days, until reaching 80% confluence as confirmed by optic microscopy observance.

4.6. Cell treatment. Complexes were initially solved on DMSO to a concentration of 20 mM and then diluted on cell culture without fetal bovine serum to the required work concentrations. For treatment, cell culture medium was replaced with medium containing complexes and cells were incubated at 37ºC for a variable time depending on the assay.

4.7. Cell proliferation assay and IC_{50} calculation. Two different methods were used to determine IC_{50}: 3-(4,5-dimethyl-2-thiazoyl)-2,5-diphenyltetrazolium bromide (MTT) assay and sulforhodamine B (SRB) assay. MTT assay was performed as previously described by Mármol *et al*. [91]; SRB assay was performed as previously described by Jiménez *et al*. [92].

For IC_{50} calculation, cells were grown in 96-wells plates at a density of 4000 cells per well and incubated overnight at standard culture conditions. Then, cells were exposed to a range of concentrations of complexes (0-20 μM for complexes **3a-d** and **4a-d**; 20-100 μM for complexes **HL-1a-d** and **HL-2a-d**) for 72h. Changes in cell proliferation were analysed by MTT or SRB and the obtained absorbance values were converted into percentage of growth inhibition. Absorbance was measured with SPECTROstar Nano (BMG Labtech).

Associated content

Supporting Information

Experimental procedures corresponding to: BSA interaction, $logD_{7.4}$, solution chemistry, measurement of COX-1/2 activity, analysis of thioredoxin reductase activity, measurement of glutathione reductase activity, analysis of total cellular oxidative stress, cell death studies, determination of caspase 3 activity and mitochondrial membrane potential, cell cycle analysis and Statistical Analysis are included in the supporting information. In addition, RMN spectra, UV-Vis spectra from stability assays, BSA fluorescence quenching spectra, calculation of IC_{50} values with the SRB technique of the gold complexes, determination of the Selectivity Index, Analysis of cell viability of differentiated Caco-2 cells, percentages of necrotic population and percentages of necrotic population are available free of charge via the Internet at http://pubs.acs.org..

Acknowledgments

Authors thank to Centro de Investigación Biomédica de Aragón (CIBA), España for technical assistance: http://www.iacs.aragon.es, use of Servicio General de Apoyo a la Investigación-SAI, Universidad de Zaragoza. We thank The Ministerio de Economia y Competitividad (CTQ2016-75816-C2-1-P and SAF2016-75441-R), CIBERobn under Grant (CB06/03/1012) of the Instituto Carlos III, European Grant Interreg/SUDOE (Redvalue, SOE1/PI/E0123) and Aragon Regional Government (B16-R17 and E07-17R) for financial support.

Highlights

- Multi-targeted mechanism of action promoted by Alkynyl Gold(I) derivatives.
- Interaction with COX-1/2 enzyme.
- Interaction with the redox enzymes TrxR and GR leading to an increased ROS production.
- Cell death *via* the intrinsic pathway and alteration of cell cycle progression.

Conflict of interest

Authors declare no conflict of interest.

Abbreviations

1,1',3,3,3'-hexamethylindodicarbo-cyanine iodide: DiIC1
1,3,5-triaza-7-phosphaadamantane: PTA
1-thio-β-D-glucopyranosatotriethylphosphane gold-2,3,4,6-tetraacetate: auranofin
3-(4,5-dimethyl-2-thiazoyl)-2,5-diphenyltetrazolium bromide: MTT
Bovine serum albumin: BSA
Chloroquine: CQ
Colorectal cancer: CRC
Cyclooxygenase: COX
Dimethylsulfoxide: DMSO
Ethylenediaminetetraacetic acid: EDTA
Food and Drug Administration: FDA
Glutathione: GSH
Glutathione reductase: GR
Human serum albumin: HSA

Mitochondrial membrane potential: MMP

Reactive oxygen species: ROS

Selectivity Index: SI

Sulforhodamine B: SRB

Thioredoxin reductase: TrxR

References

[1] E. Wong, C.M. Giandomenico, Current Status of Platinum-Based Antitumor Drugs, Chem. Rev., 99 (1999) 2451-2466.
[2] Y. Jung, S.J. Lippard, Direct Cellular Responses to Platinum-Induced DNA Damage, Chem. Rev., 107 (2007) 1387-1407.
[3] D. Wang, S.J. Lippard, Cellular processing of platinum anticancer drugs, Nat. Rev. Drug Discovery, 4 (2005) 307-320.
[4] T. Onodera, I. Momose, M. Kawada, Potential Anticancer Activity of Auranofin, Chem. Pharma. Bull., 67 (2019) 186-191.
[5] B. Englinger, C. Pirker, P. Heffeter, A. Terenzi, C.R. Kowol, B.K. Keppler, W. Berger, Metal Drugs and the Anticancer Immune Response, Chem. Rev., 119 (2019) 1519-1624.
[6] A. Bergamo, P.J. Dyson, G. Sava, The mechanism of tumour cell death by metal-based anticancer drugs is not only a matter of DNA interactions, Coord. Chem. Rev., 360 (2018) 17-33.
[7] G. Palermo, A. Magistrato, T. Riedel, T. von Erlach, C.A. Davey, P.J. Dyson, U. Rothlisberger, Fighting Cancer with Transition Metal Complexes: From Naked DNA to Protein and Chromatin Targeting Strategies, ChemMedChem, 11 (2016) 1199-1210.
[8] G. Chopra, R. Samudrala, Exploring Polypharmacology in Drug Discovery and Repurposing Using the CANDO Platform, Curr. Pharma. Design, 22 (2016) 3109 - 3123.
[9] C. Marzano, V. Gandin, A. Folda, G. Scutari, A. Bindoli, M.P. Rigobello, Inhibition of thioredoxin reductase by auranofin induces apoptosis in cisplatin-resistant human ovarian cancer cells, Free Radical Biol. Med., 42 (2007) 872-881.
[10] T. Onodera, I. Momose, M. Kawada, Potential Anticancer Activity of Auranofin, Chem. Pharm. Bull., 67 (2019) 186-191.
[11] X.N. Zhang, K. Selvaraju, A.A. Saei, P. D'Arcy, R.A. Zubarev, E.S.J. Arner, S. Linder, Repurposing of auranofin: Thioredoxin reductase remains a primary target of the drug, Biochimie, 162 (2019) 46-54.
[12] N. Liu, X. Li, H. Huang, C. Zhao, S. Liao, C. Yang, S. Liu, W. Song, X. Lu, X. Lan, X. Chen, S. Yi, L. Xu, L. Jiang, C. Zhao, X. Dong, P. Zhou, S. Li, S. Wang, X. Shi, P.Q. Dou, X. Wang, J. Liu, Clinically used antirheumatic agent auranofin is a proteasomal deubiquitinase inhibitor and inhibits tumor growth, Oncotarget, 5 (2014) 5453-5471.
[13] K. Patel, Z.S.O. Ahmed, X.M. Huang, Q.Q. Yang, E. Ekinci, C.M. Neslund-Dudas, B. Mitra, F. Elnady, Y.H. Ahn, H.J. Yang, J.B. Liu, Q.P. Dou, Discovering proteasomal deubiquitinating enzyme inhibitors for cancer therapy: lessons from rational design, nature and old drug reposition, Future Med. Chem., 10 (2018) 2087-2108.
[14] A. Arlt, I. Bauer, C. Schafmayer, J. Tepel, S.S. Muerkoster, M. Brosch, C. Roder, H. Kalthoff, J. Hampe, M.P. Moyer, U.R. Folsch, H. Schafer, Increased proteasome subunit protein expression and proteasome activity in colon cancer relate to an enhanced activation of nuclear factor E2-related factor 2 (Nrf2), Oncogene, 28 (2009) 3983-3996.
[15] R.G. Kenny, C.J. Marmion, Toward Multi-Targeted Platinum and Ruthenium Drugs—A New Paradigm in Cancer Drug Treatment Regimens?, Chem. Rev., 119 (2019) 1058-1137.

[16] E.B. Mojzer, M.K. Hrncic, M. Skerget, Z. Knez, U. Bren, Polyphenols: Extraction Methods, Antioxidative Action, Bioavailability and Anticarcinogenic Effects, Molecules, 21 (2016).
[17] C. Manach, A. Scalbert, C. Morand, C. Remesy, L. Jimenez, Polyphenols: food sources and bioavailability, Am. J. Clin. Nutr., 79 (2004) 727-747.
[18] R.J. Nijveldt, E. van Nood, D.E.C. van Hoorn, P.G. Boelens, K. van Norren, P.A.M. van Leeuwen, Flavonoids: a review of probable mechanisms of action and potential applications, Am. J. Clin. Nutr., 74 (2001) 418-425.
[19] A.F. Almeida, G.I.A. Borge, M. Piskula, A. Tudose, L. Tudoreanu, K. Valentova, G. Williamson, C.N. Santos, Bioavailability of Quercetin in Humans with a Focus on Interindividual Variation, Compr. Rev. Food Sci. F., 17 (2018) 714-731.
[20] R.V. Patel, B.M. Mistry, S.K. Shinde, R. Syed, V. Singh, H.S. Shin, Therapeutic potential of quercetin as a cardiovascular agent, Eur. J. Med. Chem., 155 (2018) 889-904.
[21] R.L. Nagula, S. Wairkar, Recent advances in topical delivery of flavonoids: A review, J. Control Release, 296 (2019) 190-201.
[22] J. Wang, X. Fang, L. Ge, F. Cao, L. Zhao, Z. Wang, W. Xiao, Antitumor, antioxidant and anti-inflammatory activities of kaempferol and its corresponding glycosides and the enzymatic preparation of kaempferol, PLOS ONE, 13 (2018) e0197563.
[23] S.G. Darband, M. Kaviani, B. Yousefi, S. Sadighparvar, F.G. Pakdel, J.A. Attari, I. Mohebbi, S. Naderi, M. Majidinia, Quercetin: A functional dietary flavonoid with potential chemo-preventive properties in colorectal cancer, J. Cell. Physicol., 233 (2018) 6544-6560.
[24] B. Butun, G. Topcu, T. Ozturk, Recent Advances on 3-Hydroxyflavone Derivatives: Structures and Properties, Mini-Review. Med. Chem., 18 (2018) 98-103.
[25] M. Asensi, A. Ortega, S. Mena, F. Feddi, J.M. Estrela, Natural polyphenols in cancer therapy, Crit. Rev. Clin. Lab. Sci., 48 (2011) 197-216.
[26] F. Perez-Vizcaino, C.G. Fraga, Research trends in flavonoids and health, Arch. Biochem. Biophys., 646 (2018) 107-112.
[27] S.C. Gupta, A.B. Kunnumakkara, S. Aggarwal, B.B. Aggarwal, Inflammation, a Double-Edge Sword for Cancer and Other Age-Related Diseases., Front. Immunol., 9 (2018) 2160.
[28] Y. Wang, W. Wang, K.Z. Sanidad, P.A. Shih, X. Zhao, G. Zhang, Eicosanoid signaling in carcinogenesis of colorectal cancer. Cancer Metastasis Rev 2018, 37 (2-3), 257-267., Cancer Metastasis Rev., 37 (2018) 257-267.
[29] M. Grazul, E. Budzisz, Biological activity of metal ions complexes of chromones, coumarins and flavones, Coord. Chem. Rev., 253 (2009) 2588-2598.
[30] P. Mladěnka, K. Macáková, T. Filipský, L. Zatloukalová, L. Jahodář, P. Bovicelli, I.P. Silvestri, R. Hrdina, L. Saso, In vitro analysis of iron chelating activity of flavonoids, J. Inorg. Biochem., 105 (2011) 693-701.
[31] A. Kurzwernhart, S. Mokesch, E. Klapproth, M.S. Adib-Ravazi, M.A. Jakupec, C.G. Hartinger, W. Kandioller, B.K. Keppler, Flavonoid-Based Organometallics with Different Metal Centers - Investigations of the Effects on Reactivity and Cytotoxicity, Eur. J. Inorg. Chem., (2016) 240-246.
[32] R. Gaur, L. Mishra, Bi-nuclear Ru(II) complexes of bis-chalcone and bis-flavonol: synthesis, characterization, photo cleavage of DNA and Topoisomerase I inhibition, RSC Advances, 3 (2013) 12210-12219.
[33] A. Kurzwernhart, W. Kandioller, S. Bachler, C. Bartel, S. Martic, M. Buczkowska, G. Muhlgassner, M.A. Jakupec, H.B. Kraatz, P.J. Bednarski, V.B. Arion, D. Marko, B.K. Keppler, C.G. Hartinger, Structure-Activity Relationships of Targeted Ru-II(eta(6)-p-Cymene) Anticancer Complexes with Flavonol-Derived Ligands, J. Med. Chem., 55 (2012) 10512-10522.
[34] N. Mirzadeh, S.H. Priver, A. Abraham, R. Shukla, V. Bansal, S.K. Bhargava, Linking Flavonoids to Gold - A New Family of Gold Compounds for Potential Therapeutic Applications, Eur. J. Inorg. Chem., (2015) 4275-4279.

[35] E. Cerrada, V. Fernández-Moreira, M.C. Gimeno, Gold and platinum alkynyl complexes for biomedical applications., in: P. Pérez (Ed.) Advances in Organometallic Chemistry, Elsevier Academic Press, 2019, pp. 227-258.
[36] H.T. Liu, X.G. Xiong, P.D. Dau, Y.L. Wang, D.L. Huang, J. Li, L.S. Wang, Probing the nature of gold-carbon bonding in gold-alkynyl complexes, Nat. Commun, 4:2223 doi: 10.1038/ncomms3223 (2013).
[37] S. Gunduz, A.C. Goren, T. Ozturk, Facile Syntheses of 3-Hydroxyflavones, Organic Lett., 14 (2012) 1576-1579.
[38] D. Li, X. Hong, C.-M. Che, W.-C. Lo, S.-M. Peng, Luminescent gold(I) acetylide complexes. Photophysical and photoredox properties and crystal structure of [{Au(CCPh)}$_2$(μ-$Ph_2PCH_2CH_2PPh_2$)], J. Chem. Soc. Dalton Trans., (1993) 2929-2932.
[39] C.K. Lee, T. Uchida, K. Kitagawa, A. Yagi, N.S. Kim, S. Goto, Relationship between lipophilicity and skin permeability of various drugs from an ethanol/water/lauric acid system, Biol. Pharm. Bull., 17 (1994) 1421-1424.
[40] E. García-Moreno, E. Cerrada, M.J. Bolsa, A. Luquin, M. Laguna, Water-Soluble Phosphanes Derived from 1,3,5-Triaza-7-phosphaadamantane and Their Reactivity towards Gold(I) Complexes, Eur. J. Inorg. Chem., (2013) 2020-2030.
[41] F. Menaa, A. Menaa, B. Menaa, Chapter 65 - Polyphenols Nano-Formulations for Topical Delivery and Skin Tissue Engineering, in: R.R. Watson, V.R. Preedy, S. Zibadi (Eds.) Polyphenols in Human Health and Disease, Academic Press, San Diego, 2014, pp. 839-848.
[42] D. Carter, J.X. Ho, Advances in Protein Chemistry, Academic Press, New York, 1994.
[43] J.R. Lakowicz, in 'Principles of fluorescence Spectroscopy', Springer, Baltimore, Maryland, USA, 2006.
[44] H. Polet, J. Steinhardt, Binding-induced alterations in ultraviolet abssorption of native serum albumin, Biochemistry, 7 (1968) 1348-1356.
[45] J.A. Molina-Bolivar, F. Galisteo-Gonzalez, C.C. Ruiz, M.M.O. Donnell, A. Parra, Spectroscopic investigation on the interaction of maslinic acid with bovine serum albumin, J. Lumin., 156 (2014) 141-149.
[46] J. Quero, S. Cabello, T. Fuertes, I. Marmol, R. Laplaza, V. Polo, M.C. Gimeno, M.J. Rodriguez-Yoldi, E. Cerrada, Proteasome versus Thioredoxin Reductase Competition as Possible Biological Targets in Antitumor Mixed Thiolate-Dithiocarbamate Gold(III) Complexes, Inorg. Chem., 57 (2018) 10832-10845.
[47] I.M. Cristina Sánchez-de-Diego, Rocío Pérez, Sonia Gascón, Mª Jesús Rodriguez-Yoldi and Elena Cerrada, The anticancer effect related to disturbances in redox balance on Caco-2 cells caused by an alkynyl gold(I) complex, J. Inorg. Biochem., 166 (2017) 108-121.
[48] E. Atrian-Blasco, S. Gascon, M.J. Rodriguez-Yoldi, M. Laguna, E. Cerrada, Novel Gold(I) Thiolate Derivatives Synergistic with 5-Fluorouracil as Potential Selective Anticancer Agents in Colon Cancer, Inorg. Chem., 56 (2017) 8562-8579.
[49] E. Garcia-Moreno, A. Tomas, E. Atrian-Blasco, S. Gascon, E. Romanos, M.J. Rodriguez-Yoldi, E. Cerrada, M. Laguna, In vitro and in vivo evaluation of organometallic gold(I) derivatives as anticancer agents, Dalton Trans., 45 (2016) 2462-2475.
[50] I. Marmol, M. Virumbrales-Munoz, J. Quero, C. Sanchez-De-Diego, L. Fernandez, I. Ochoa, E. Cerrada, M.J.R. Yoldi, Alkynyl gold(I) complex triggers necroptosis via ROS generation in colorectal carcinoma cells, J. Inorg. Biochem., 176 (2017) 123-133.
[51] E. Garcia-Moreno, S. Gascon, M.J. Rodriguez-Yoldi, E. Cerrada, M. Laguna, S-Propargylthiopyridine Phosphane Derivatives As Anticancer Agents: Characterization and Antitumor Activity, Organometallics, 32 (2013) 3710-3720.
[52] E. Garcia-Moreno, S. Gascon, E. Atrian-Blasco, M.J. Rodriguez-Yoldi, E. Cerrada, M. Laguna, Gold(I) complexes with alkylated PTA (1,3,5-triaza-7-phosphaadamantane) phosphanes as anticancer metallodrugs, Eur. J. Med. Chem., 79 (2014) 164-172.
[53] E. García-Moreno, S. Gascón, J.A.G.d. Jalón, E. Romanos, M.J. Rodriguez-Yoldi, E. Cerrada, M. Laguna, In vivo anticancer activity, toxicology and histopathological studies of the thiolate

gold(I) complex [Au(Spyrimidine)(PTA-CH2Ph)]Br, Anti-Cancer Agents Med. Chem., 15 (2015) 773-782.
[54] g. Sudlow, d.J. Birkett, d.N. Wade, Further Characterization of Specific Drug Binding Sites on Human Serum Albumin, Mol. Pharmacol., 12 (1976) 1052-1061.
[55] G.W. Zhang, Y.D. Ma, Mechanistic and conformational studies on the interaction of food dye amaranth with human serum albumin by multispectroscopic methods, Food Chem., 136 (2013) 442-449.
[56] P. Wang, S.M. Henning, D. Heber, Limitations of MTT and MTS-based assays for measurement of antiproliferative activity of green tea polyphenols, PLoS One, 5 (2010) e10202.
[57] R.G. Balasingham, C.F. Williams, H.J. Mottram, M.P. Coogan, S.J.A. Pope, Gold(I) Complexes Derived from Alkynyloxy-Substituted Anthraquinones: Syntheses, Luminescence, Preliminary Cytotoxicity, and Cell Imaging Studies, Organometallics, 31 (2012) 5835-5843.
[58] A. Meyer, C.P. Bagowski, M. Kokoschka, M. Stefanopoulou, H. Alborzinia, S. Can, D.H. Vlecken, W.S. Sheldrick, S. Wolfl, I. Ott, On the Biological Properties of Alkynyl Phosphine Gold(I) Complexes, Angew. Chem. Int. Edit., 51 (2012) 8895-8899.
[59] B. Bertrand, A. Casini, A golden future in medicinal inorganic chemistry: the promise of anticancer gold organometallic compounds, Dalton Trans., 43 (2014) 4209-4219.
[60] C. Sanchez-de-Diego, I. Marmol, R. Perez, S. Gascon, M.J. Rodriguez-Yoldi, E. Cerrada, The anticancer effect related to disturbances in redox balance on Caco-2 cells caused by an alkynyl gold(I) complex, J. Inorg. Biochem., 166 (2017) 108-121.
[61] R.B. Badisa, S.F. Darling-Reed, P. Joseph, J.S. Cooperwood, L.M. Latinwo, C.B. Goodman, Selective cytotoxic activities of two novel synthetic drugs on human breast carcinoma MCF-7 cells, Anticancer Res, 29 (2009) 2993-2996.
[62] K. Vidyalakshmi, P. Kamalakannan, S. Viswanathan, S. Ramaswamy, Anti-inflammatory effect of certain dihydroxy flavones and the mechanisms involved, Antiinflamm Antiallergy Agents Med Chem, 11 (2012) 253-261.
[63] R.J. Meshram, K.T. Bagul, S.P. Pawnikar, S.H. Barage, B.S. Kolte, R.N. Gacche, Known compounds and new lessons: structural and electronic basis of flavonoid-based bioactivities, J Biomol Struct Dyn, (2019) 1-17.
[64] H.S. Youn, J.Y. Lee, S.I. Saitoh, K. Miyake, D.H. Hwang, Auranofin, as an anti-rheumatic gold compound, suppresses LPS-induced homodimerization of TLR4, Biochem. Biophys. Res. Comm., 350 (2006) 866-871.
[65] I. Ott, T. Koch, H. Shorafa, Z. Bai, D. Poeckel, D. Steinhilber, R. Gust, Synthesis, cytotoxicity, cellular uptake and influence on eicosanoid metabolism of cobalt-alkyne modified fructoses in comparison to auranofin and the cytotoxic COX inhibitor Co-ASS, Org Biomol Chem, 3 (2005) 2282-2286.
[66] S. Roscales, N. Bechmann, D.H. Weiss, M. Kockerling, J. Pietzsch, T. Kniess, Novel valdecoxib derivatives by ruthenium(ii)-promoted 1,3-dipolar cycloaddition of nitrile oxides with alkynes - synthesis and COX-2 inhibition activity, Medchemcomm, 9 (2018) 534-544.
[67] G. Rubner, K. Bensdorf, A. Wellner, B. Kircher, S. Bergemann, I. Ott, R. Gust, Synthesis and biological activities of transition metal complexes based on acetylsalicylic acid as neo-anticancer agents, J Med Chem, 53 (2010) 6889-6898.
[68] U.S. Akarca, Gastrointestinal effects of selective and non-selective non-steroidal anti-inflammatory drugs, Curr Pharm Des, 11 (2005) 1779-1793.
[69] S.H. Bae, E.S. Jung, Y.M. Park, B.S. Kim, B.K. Kim, D.G. Kim, W.S. Ryu, Expression of cyclooxygenase-2 (COX-2) in hepatocellular carcinoma and growth inhibition of hepatoma cell lines by a COX-2 inhibitor, NS-398, Clin Cancer Res, 7 (2001) 1410-1418.
[70] H. Kamitani, M. Geller, T. Eling, Expression of 15-lipoxygenase by human colorectal carcinoma Caco-2 cells during apoptosis and cell differentiation, J Biol Chem, 273 (1998) 21569-21577.

[71] E. Half, X.M. Tang, K. Gwyn, A. Sahin, K. Wathen, F.A. Sinicrope, Cyclooxygenase-2 expression in human breast cancers and adjacent ductal carcinoma in situ, Cancer Res, 62 (2002) 1676-1681.
[72] Y. Cheng, Y. Qi, Current Progresses in Metal-based Anticancer Complexes as Mammalian TrxR Inhibitors, Anticancer Agents Med Chem, 17 (2017) 1046-1069.
[73] A. Bindoli, M.P. Rigobello, G. Scutari, C. Gabbiani, A. Casini, L. Messori, Thioredoxin reductase: A target for gold compounds acting as potential anticancer drugs, Coord. Chem. Rev., 253 (2009) 1692-1707.
[74] N. Couto, J. Wood, J. Barber, The role of glutathione reductase and related enzymes on cellular redox homoeostasis network, Free Radic Biol Med, 95 (2016) 27-42.
[75] X. Yan, X. Zhang, L. Wang, R. Zhang, X. Pu, S. Wu, L. Li, P. Tong, J. Wang, Q.H. Meng, V.B. Jensen, L. Girard, J.D. Minna, J.A. Roth, S.G. Swisher, J.V. Heymach, B. Fang, Inhibition of Thioredoxin/Thioredoxin Reductase Induces Synthetic Lethality in Lung Cancers with Compromised Glutathione Homeostasis, Cancer Res, 79 (2019) 125-132.
[76] Y. Du, H. Zhang, J. Lu, A. Holmgren, Glutathione and glutaredoxin act as a backup of human thioredoxin reductase 1 to reduce thioredoxin 1 preventing cell death by aurothioglucose, J Biol Chem, 287 (2012) 38210-38219.
[77] J. Lu, L.V. Papp, J. Fang, S. Rodriguez-Nieto, B. Zhivotovsky, A. Holmgren, Inhibition of Mammalian thioredoxin reductase by some flavonoids: implications for myricetin and quercetin anticancer activity, Cancer Res, 66 (2006) 4410-4418.
[78] K. Zhang, E.B. Yang, W.Y. Tang, K.P. Wong, P. Mack, Inhibition of glutathione reductase by plant polyphenols, Biochem Pharmacol, 54 (1997) 1047-1053.
[79] E. Jortzik, M. Farhadi, R. Ahmadi, K. Toth, J. Lohr, B.M. Helmke, S. Kehr, A. Unterberg, I. Ott, R. Gust, V. Deborde, E. Davioud-Charvet, R. Reau, K. Becker, C. Herold-Mende, Antiglioma activity of GoPI-sugar, a novel gold(I)-phosphole inhibitor: chemical synthesis, mechanistic studies, and effectiveness in vivo, Biochim Biophys Acta, 1844 (2014) 1415-1426.
[80] I. Villegas, M.J. Martin, C. La Casa, V. Motilva, C.A. De La Lastra, Effects of oxicam inhibitors of cyclooxygenase on oxidative stress generation in rat gastric mucosa. A comparative study, Free Radic Res, 36 (2002) 769-777.
[81] C. Nicco, F. Batteux, ROS Modulator Molecules with Therapeutic Potential in Cancers Treatments, Molecules, 23 (2017).
[82] M. Altaf, N. Casagrande, E. Mariotto, N. Baig, A.N. Kawde, G. Corona, R. Larcher, C. Borghese, C. Pavan, A.A. Seliman, D. Aldinucci, A.A. Isab, Potent In Vitro and In Vivo Anticancer Activity of New Bipyridine and Bipyrimidine Gold (III) Dithiocarbamate Derivatives, Cancers, 11 (2019) 14.
[83] M.W. Sung, D.Y. Lee, S.W. Park, S.M. Oh, J.J. Choi, E.S. Shin, S.K. Kwon, S.H. Ahn, Y.H. Kim, Celecoxib enhances the inhibitory effect of 5-FU on human squamous cell carcinoma proliferation by ROS production, Laryngoscope, 127 (2017) E117-E123.
[84] J.N. Boodram, I.J. McGregor, P.M. Bruno, P.B. Cressey, M.T. Hemann, K. Suntharalingam, Breast Cancer Stem Cell Potent Copper(II)-Non-Steroidal Anti-Inflammatory Drug Complexes, Angew Chem Int Ed Engl, 55 (2016) 2845-2850.
[85] B.T. Elie, J. Fernández-Gallardo, N. Curado, M.A. Cornejo, J.W. Ramos, M. Contel, Bimetallic titanocene-gold phosphane complexes inhibit invasion, metastasis, and angiogenesis-associated signaling molecules in renal cancer, Eur. J. Med. Chem., 161 (2019) 310-322.
[86] H. Zhou, M. Yuan, Q. Yu, X. Zhou, W. Min, D. Gao, Autophagy regulation and its role in gastric cancer and colorectal cancer, Cancer Biomark, 17 (2016) 1-10.
[87] Y. Shi, B. Tang, P.W. Yu, B. Tang, Y.X. Hao, X. Lei, H.X. Luo, D.Z. Zeng, Autophagy protects against oxaliplatin-induced cell death via ER stress and ROS in Caco-2 cells, PLoS One, 7 (2012) e51076.

[88] Z. Assefa, B.G. McBurnett, R.J. Staples, J.P. Fackler, Structures and spectroscopic properties of gold(i) complexes of 1,3,5-triaza-7-phosphaadamantane (tpa) .2. Multiple-state emission from (tpa)aux (x=cl, br, i) complexes, Inorg. Chem., 34 (1995) 4965-4972.
[89] C.A. McAuliffe, R.V.D. Parish, P.D. Randall, Gold(I) complexes of unidentate and bidentate phosphorus-, arsenic-, antimony-, and sulphur-donor ligands, J. Chem. Soc., Dalton Trans., (1979) 1730-1735.
[90] G. Sheldrick, Crystal structure refinement with SHELXL, Acta Cryst. Section C, 71 (2015) 3-8.
[91] I. Marmol, M. Virumbrales-Munoz, J. Quero, C. Sanchez-de-Diego, L. Fernandez, I. Ochoa, E. Cerrada, M.J.R. Yoldi, Alkynyl gold(I) complex triggers necroptosis via ROS generation in colorectal carcinoma cells, J Inorg Biochem, 176 (2017) 123-133.
[92] S. Jimenez, S. Gascon, A. Luquin, M. Laguna, C. Ancin-Azpilicueta, M.J. Rodriguez-Yoldi, Rosa canina Extracts Have Antiproliferative and Antioxidant Effects on Caco-2 Human Colon Cancer, PLoS One, 11 (2016) e0159136.

Synopsis

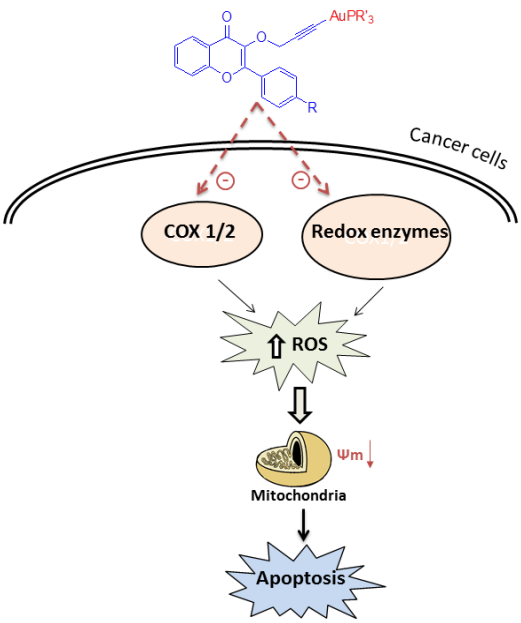

Targeted therapies for cancer treatment have revolutionized the concept of oncological medicine. However, the single-target therapy is vanishing in favour of a multi-target approach, where new drugs are able to simultaneously target different molecules. Here we describe new alkynyl gold(I) phosphane complexes derived from 3-hydroxyflavones, whose mechanism of action involves cell death via two independent targets.